International Journal of Earth Sciences (2025) 114:1029–1050
https://doi.org/10.1007/s00531-025-02528-9

REVIEW ARTICLE

Geometrical analysis of the 3-D structure of the western Tauern Window (European Eastern Alps)

J. Rudmann[1,2] · D. C. Tanner[1] · M. Stipp[2] · H. Pomella[3] · C. Brandes[4]

Received: 7 March 2025 / Accepted: 16 July 2025 / Published online: 12 August 2025

Abstract

The Tauern Window (TW) in the European Eastern Alps is one of the most prominent tectonic windows on earth. Deeper structural levels of the orogenic wedge are almost completely exposed, which is why complex collisional deformation processes, including indenter tectonics, can be studied. Although the TW has been investigated over decades, its present-day, 3-D geometry is not completely deciphered. However, it provides insights into its Miocene deformation history, which is still debated. The latter was driven by indentation tectonics, which heavily shaped the structure of the TW, especially its western part. The aim of this study is to infer the Miocene deformation history from the present-day, 3-D structure of the upper crust of the western TW and to relate it to possible deeper crustal deformation processes. For the first time, we uncover the large-scale structure of the western TW, including two end-member models of the viscous Brenner normal fault by constructing a 3-D model using the software MOVE™. Our model reveals that the south-vergence of the large-scale antiforms increases in westerly direction and their cylindricity decreases in southern direction, thus, towards the front of the Dolomites indenter. Protruding middle and lower crust of the Dolomites indenter below the area of the TRANSALP seismic section could be responsible, also for the westward plunge of the entire western TW, which might have favoured the development of the Brenner normal fault. The Schöberspitzen antiform likely developed pre- or synkinematically to the westward plunge of the western TW, thus during the Miocene.

Keywords Modelling · Tauern Window · Eastern Alps · Indentation · Deformation

Introduction

The Tauern Window in the European Eastern Alps is one of the largest and best-studied tectonic windows on Earth (Fig. 1a). The deformation history of the complex-folded units of the Tauern Window began in the Early Cenozoic era: The convergence of the Adriatic Plate and the southward subduction of the Penninic Ocean and the European continental margin (Subpenninic) led finally to the collision between the European Plate (lower plate) and the Adriatic Plate (upper plate; e.g., Froitzheim et al. 1994; Handy et al. 2010; Schmid et al. 2004). Rocks of the Penninic Oceanic crust and the Subpenninic were subducted to depths up to ca. 65 km (e.g., Dachs 1986, 1990; Hoschek 2001, 2004) and subsequently, nappe stacking and duplexing in the orogenic wedge initiated (e.g., Schmid et al. 2013 and references therein). In the Late Oligocene/Early Miocene, shortening, initially accommodated by collisional accretion, was replaced by upright (re-)folding of the nappe stack caused by the northward indentation of the Dolomites indenter (e.g., Ratschbacher et al. 1991a, b; Lammerer and Weger 1998; Frisch et al. 2000; Linzer et al. 2002; Rosenberg et al. 2004, 2007, 2018; Stipp et al. 2004; Pomella et al. 2011, 2012; Scharf et al. 2013; Schmid et al. 2013; Favaro et al. 2017; Ricchi et al. 2020; Verwater et al. 2021; McPhee and Handy 2024; Handy 2025). The Miocene N-S-shortening in front of the Dolomites indenter was accompanied by contemporaneous W-E-extension, including orogeny-parallel normal faulting at the eastern and western end of the Tauern

✉ J. Rudmann
Julia.Rudmann@liag-institut.de; julia.rudmann@gmx.de

1 LIAG Institute for Applied Geophysics, Stilleweg 2, 30655 Hannover, Germany

2 Martin Luther University Halle-Wittenberg, Von-Seckendorff-Platz 3, 06120 Halle/Saale, Germany

3 University of Innsbruck, Innrain 52F, 6020 Innsbruck, Austria

4 Leibniz University Hannover, Callinstr. 30, 30167 Hannover, Germany

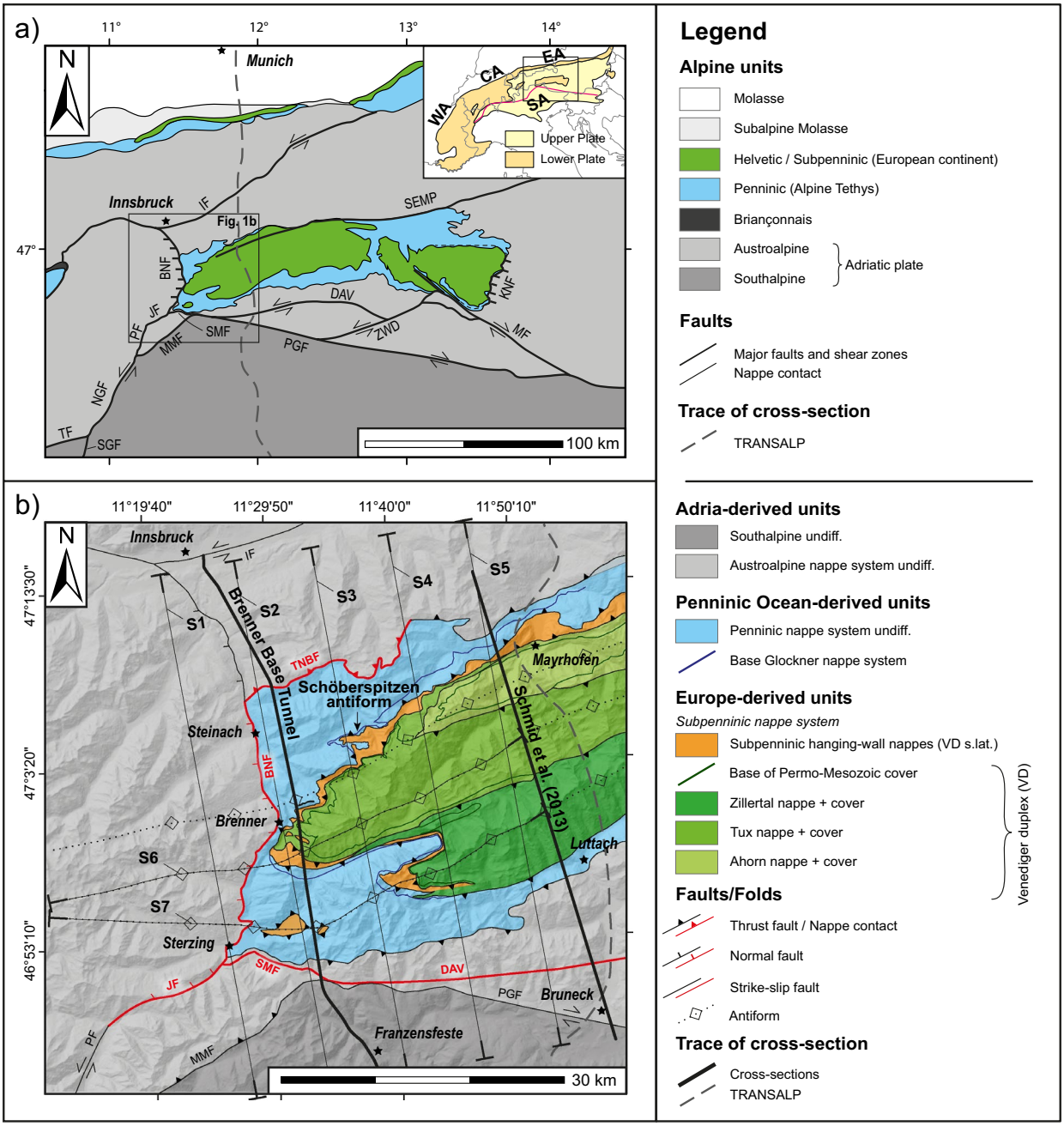

Fig. 1 **a** Tectonic overview map of the Tauern Window and the Eastern Alps (modified after Schmid et al. 2004 and Rosenberg et al. 2015). Upper right corner: Tectonic overview map of the European Alps, modified after Ortner et al. (2006) and McPhee and Handy (2024). Grey lines are country borders. Magenta line: Periadriatic fault system. Lower Plate: Helvetic/Subpenninic and Penninic derived. Upper Plate: Adria derived. *CA* Central Alps, *EA* Eastern Alps, *SA* Southern Alps, *WA* Western Alps. **b** Compiled and simplified tectonic map of the western Tauern Window (based on maps listed in section "Map compilation and structural data analysis". Thin black lines (S1–S7) show the location of newly constructed cross-sections in this work through the final 3-D model (see Fig. 8). Fault abbreviations in **a** and **b**: *BNF* Brenner normal fault, *DAV* Defereggen Antholz Vals fault, *IF* Inntal fault, *JF* Jaufen fault, *KNF* Katschberg normal fault, *MF* Mölltal fault, *MMF* Meran Mauls fault, *NGF* Northern Giudicarie fault, *PGF* Pustertal Gailtal fault, *PF* Passeier fault, *SGF* Southern Giudicarie fault, *SEMP* Salzach Ennstal Mariazell Puchberg fault, *SMF* Sterzing Mauls fault, *TF* Tonale Fault, *ZWD* Zwischenbergen Wöllatratten Drau fault, *TNBF* Tauern northern boundary fault. Bold red lines show faults that are relevant to the model with respect to the viscous Brenner normal fault and its possible northern and southern continuation

Window (Katschberg normal fault and Brenner normal fault; e.g., Selverstone 1988; Behrmann 1988; Axen et al. 1995; Fügenschuh et al. 1997, 2012; Frisch et al. 2000; Rosenberg and Garcia 2011, 2012; Scharf et al. 2013; Wolff et al. 2020, 2021, 2024; Wölfler et al. 2023; Fig. 1a) and lateral extrusion towards the east along major strike-slip faults, like the Inntal fault, the Salzach–Ennstal–Mariazell–Puchberg (SEMP) fault, the Mölltal fault and the Pustertal Gailtal fault (Fig. 1; e.g., Ratschbacher et al. 1991a, b; Frisch et al. 2000; Linzer et al. 2002; Rosenberg et al. 2018 and references therein; McPhee and Handy 2024; Handy 2025). The previously-described tectonic processes, in combination with erosion, exhumed and denuded the structure and the associated rocks of the usually deep-seated orogenic wedge. The Tauern Window is therefore unique, because deeper structural levels of the orogenic wedge are almost completely preserved and exposed. In particular, its western end is a key area to examine indenter tectonics (Fig. 1). Although, numerous studies have been carried out about this topic (e.g., Ratschbacher et al. 1991a, b; Frisch et al. 2000; Linzer et al. 2002; Rosenberg et al. 2004, 2007, 2018; Rosenberg and Schneider 2008; Pomella et al. 2011, 2012; Schmid et al 2013; McPhee and Handy 2024; Handy 2025), it remains a matter of debate, how indentation took place (e.g., indentation direction, rigid or dynamic). A new geological interpretation of seismic tomography data (McPhee and Handy 2024) reveal thickening of the lower crust below the nappes of the Tauern Window in the vicinity of the TRANSALP seismic section (TRANSALP Working Group 2002; Lüschen et al. 2004, 2006; Fig. 1). This does not occur below the westernmost Tauern Window in the vicinity of the trace of the Brenner Base Tunnel (which is currently under construction; Fig. 1; Töchterle et al. 2007; Brandner et al. 2008a), but southwest of it in the southwestern corner of the Tauern Window and mainly below the Dolomits indenter. McPhee and Handy (2024) interpret the thickening in the vicinity of the TRANSALP seismic section as middle and lower crustal detachment of the Dolomites indenter, which wedges below the Tauern Window in this area.

Interestingly, the upper crustal structure of the western Tauern Window also changes laterally over a short distance in this area. While in the westernmost Tauern Window, along the trace of the Brenner Base Tunnel, (Töchterle et al. 2007; Brandner et al. 2008a), tight, south-vergent folds occur, ca. 25 km further east, in the vicinity of the TRANSALP seismic section (TRANSALP Working Group 2002; Lüschen et al. 2004, 2006; Fig. 1), the folds become upright and their interlimb angles increase (Figs. 1b, 2; Lammerer et al. 2008; Schmid et al. 2013; Rosenberg et al. 2018). Although cross-sections (e.g., Frisch 1968, 1977; Prey 1980; Ortner et al. 2006; Töchterle et al. 2007; Lammerer et al. 2008; Veselá and Lammerer 2008; Schmid et al. 2013; Rosenberg et al. 2015; Reiter et al. 2018; Veselá et al. 2022) and 3-D models of parts of the western Tauern Window (e.g., Bistacchi et al. 2008) exist, the complete structure of this area is far from being completely understood.

The aim of this study is to present a static 3-D model of the large-scale structure of the entire western Tauern Window, and to examine whether this structure can be correlated with the previously described interpretation of McPhee and Handy (2024) of an intermediate crustal detachment of the Dolomites indenter. The 3-D model also includes the viscous Brenner normal fault and two debated end-member models of its southern continuation (e.g., Fügenschuh et al. 1997, 2012; Rosenberg and Garcia 2011, 2012). We used all available data of the area (maps, cross-sections, structural data; see section "Database and methods" and Data availability statement) and made use of inter- and extrapolating methods contained within the software MOVE™. We structurally analysed our final model, present new cross-sections, both planar in NNW-SSE direction and along the trace of the fold axes, and interrelate the upper crustal deformation of the western Tauern Window with the aforementioned new interpretation of lower crustal dynamics of the Dolomites indenter.

Geological setting

Tectonic history

In the following we focus on the Miocene deformation history (indenter phase), which is largely responsible for the shape of the present structure of the western Tauern Window, particularly its western end.

The indenter phase is characterised by the northward push of the Dolomites indenter. The Dolomites indenter, which is the eastern domain of the Adriatic indenter (e.g., Frisch et al. 2000; Rosenberg et al. 2007; Fig. 1), is located south of the Tauern Window. It is bounded by the Periadriatic fault system, which comprises the Giudicarie fault system to the west and northwest (consisting of a southern and northern segment, and the Meran Mauls fault; Fig. 1) and the Pustertal Gailtal fault to the northeast (Fig. 1). The N(NW)-directed movement of the Dolomites indenter (e.g., Fügenschuh et al. 1997; Eizenhöfer et al. 2023; Favaro et al. 2017; Laubscher 1971; Linzer et al. 2002; Mancktelow et al. 2001; McPhee and Handy 2024; Pennacchioni and Mancktelow 2007; Scharf et al. 2013; Schmid et al. 1996, 2013; Schmid and Kissling 2000; Le Breton et al. 2017; Verwater et al. 2021; Villani et al. 2024) during the Late Oligocene and Miocene (e.g., Pomella et al. 2011, 2012; Schmid et al. 2013 and references therein) caused approximately 75 km sinistral offset of the Periadric fault system along the Giudicarie fault system (e.g., Favaro et al. 2017 and references therein; Verwater et al. 2021), and modified the early Cenozoic

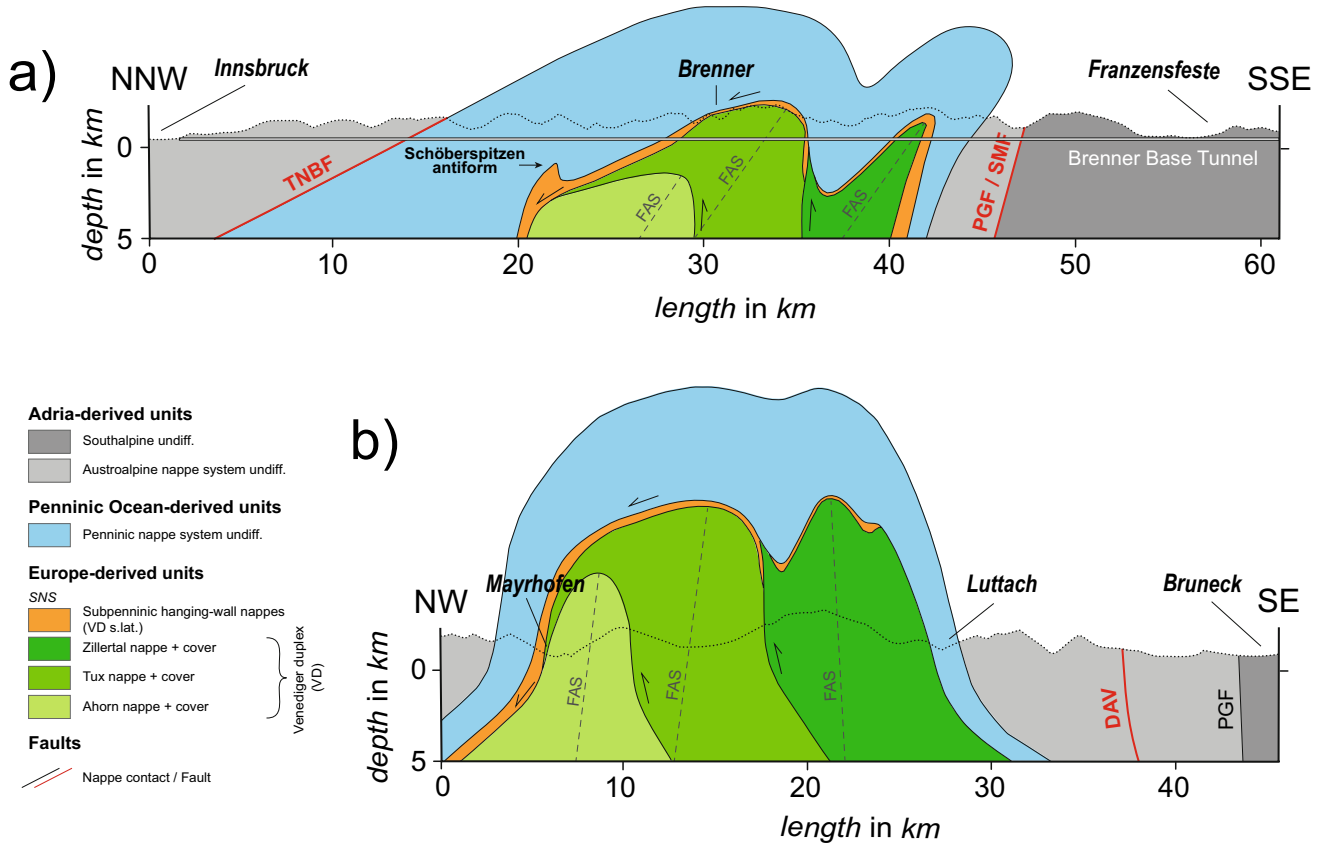

Fig. 2 Cross-sections through the western Tauern Window that were used as a basis for the 3-D model. **a** Brenner Base Tunnel section (simplified after Töchterle et al. 2007 and Rosenberg and Garcia 2011, 2012). Two models have been proposed to show the thicknesses of the Penninic and Austroalpine nappes above the today's topography, depending on the influence of the Brenner normal fault (Fügenschuh et al. 1997, 2012; Rosenberg and Garcia 2011, 2012; Schmid et al. 2013). Both models are compatible for our model since the uppermost surface of our model is the base of the Penninic nappe system (see section "Database and methods" for more details), the geometry of which is nearly the same in both models. b) Simplified cross-section of Schmid et al. (2013) near the TRANSALP seismic section (TRANSALP Working Group 2002; Lüschen et al. 2004, 2006). Approximate fault axial surfaces (FAS) are shown as grey dashed lines. Fault abbreviations: *DAV* Defereggen Antholz Vals fault, *PGF* Pustertal Gailtal fault, *SMF* Sterzing Mauls fault, *TNBF* Tauern northern boundary fault

nappe structure of the Eastern Alps (e.g., Selverstone 1985; Ratschbacher et al. 1991a, b; Frisch et al. 2000; Linzer et al. 2002; Rosenberg et al. 2004, 2007, 2018; Stipp et al. 2004; Pomella et al. 2011, 2012; Scharf et al. 2013; Schmid et al. 2013; Favaro et al. 2017; Ricchi et al. 2020; McPhee and Handy 2024; Handy 2025). The highest amount of shortening occurred in the westernmost Tauern Window in front of the tip of the Dolomites indenter (Fig. 1; e.g., Schmid et al. 2013 and references therein; Rosenberg et al. 2018 and references therein; Rudmann et al. 2025).

During the Early Miocene, shortening was first accommodated by upright-folding of the orogenic wedge, and subsequently by northward displacement of the entire Subpenninic (Europe-derived units), Penninic (Penninic Ocean-derived units) and Austroalpine (Adria-derived units) nappe stack along the Sub-Tauern ramp (e.g,. Lammerer and Weger 1998; Lammerer et al. 2008; Rosenberg et al. 2018 and references therein; McPhee and Handy 2024; Rudmann et al. 2025). At the same time, orogen-parallel extension took place, including normal faulting and lateral extrusion to the east, which partly compensated the north–south shortening. There are large normal faults perpendicular to the orogen-strike, which delimit the Tauern Window to the east and west, respectively, i.e. the Katschberg normal fault and the Brenner normal fault (Fig. 1a; e.g., Selverstone 1988; Behrmann 1988; Axen et al. 1995; Fügenschuh et al. 1997, 2012; Frisch et al. 2000; Rosenberg and Garcia 2011, 2012; Scharf et al. 2013; Wolff et al. 2020, 2021, 2024; Wölfler et al. 2023). Along-strike extrusion took place along major strike-slip faults, such as the Inntal fault, the Salzach–Ennstal–Mariazell–Puchberg (SEMP) fault in the north and the Mölltal fault, and the Pustertal Gailtal fault in the south (Fig. 1; e.g., Ratschbacher et al. 1991a, b; Frisch et al. 2000; Linzer et al. 2002; Rosenberg et al. 2018 and

references therein; McPhee and Handy 2024; Handy 2025). McPhee and Handy (2024) and Handy (2025) suggest that the aforementioned strike-slip faults north and south of the Tauern Window flatten, converge and merge below the Tauern Window forming an additional sub-horizontal extrusion surface below the Tauern Window.

Major tectonic units

The western Tauern Window comprises two major nappe systems. The Subpenninic nappe system is the structurally lower system and comprises rocks derived from the European continental margin. The Penninic nappe system is the structurally higher system, and consists of rocks derived from the Penninic Ocean (Figs.1b, 2). The Subpenninic Venediger duplex belongs to the Subpenninic nappe system and forms the core of the western Tauern Window. It consists of at least three nappes (named "gneiss cores" in the general literature), which are, from structural lowest to highest, the Ahorn nappe, the Tux nappe and the Zillertal nappe (Figs. 1b, 2; e.g., Frisch 1977; Lammerer and Weger 1998; Brandner et al. 2008a; Lammerer et al. 2008; Schmid et al. 2013; Reiter et al. 2018; Eizenhöfer et al. 2023). The nappes of the Venediger duplex mainly originated from pre-Alpine meta-plutonites (335–292 Ma; e.g., Veselá et al. 2010 and references therein). At some locations, relicts of the host rock into which the plutons intruded, are still present ("Altes Dach"; Frasl 1958). The nappes are covered and separated from each other by autochthonous Permo-Mesozoic metasediments (e.g., Fig. 1b; Frisch 1974; Veselá and Lammerer 2008; Veselá et al. 2008, 2010, 2022). During the Cenozoic Alpine Orogeny, in the course of nappe stacking, parts of these metasediments were detached from the basement, stacked and in many places isoclinally folded. Nowadays, they form nappes on top of the autochthonous cover that remained attached to the basement (Frisch 1974, 1980; Thiele 1980; Lammerer 1986; Rockenschaub et al. 2003; Töchterle et al. 2007, 2011; Lammerer et al. 2008; Veselá and Lammerer 2008; Veselá et al. 2022). In this work, we call them "Subpenninic hanging-wall nappes" and attribute them to the Venediger duplex *s. lat.* (Figs. 1b, 2).

The base of the Penninic nappe system comprises (Permo-)Triassic units (Fig. 1b; Frisch 1974; Töchterle et al. 2007, 2011; Brandner et al. 2008a, b). Some authors ascribe these units to the "Modereck nappe system" (e.g., Rockenschaub et al. 2003; Schmid et al. 2013 and references therein), whose existence is proven in the central Tauern Window (Groß et al. 2020, 2021, 2022). In the western Tauern Window, however, several authors (Staub 1924; Töchterle et al. 2007, 2011; Brandner et al. 2008a, b) claim that there is no tectonic boundary with the overlying Glockner nappe system. We follow these authors and therefore attribute these (Permo-)Triassic units to the Penninic nappe system, representing its base. Above these units, calcareous to non-calcareous schists ("Bündnerschiefer" in Glockner facies; Frasl and Frank 1966), as well as ophiolites (e.g., Höck and Koller 1989; Koller and Prestal 2003; Rockenschaub et al. 2003 and references therein; Schmid et al. 2013) of the Glockner nappe system follow. A tectonic mélange zone separates the Tauern Window from its Austroalpine frame ("Matrei Nordrahmen zone"; e.g., Koller and Prestal 2003; Rockenschaub et al. 2003 and references therein; Töchterle et al. 2007; Brandner et al. 2008a, c). This mélange consists of Lower Austroalpine lenses intermingled with "Bündnerschiefer".

Geometry of the western Tauern Window

Schmid et al. (2013) analysed the overall structure of the Tauern Window and its lateral variation along-strike. Their cross-sections through the western Tauern Window (Fig. 2) show that upright folds in the east (close to the TRANSALP seismic section; Fig. 1b; TRANSALP Working Group 2002; Lüschen et al. 2004, 2006; Lammerer et al. 2008) turn into tighter, south-vergent folds at the western end of the Tauern Window, in parts even overturned (Zillertal antiform; Rudmann et al. 2025; see also Figs. 1b, 2). In the west, the northern limb of the Tux nappe comprises a higher-order fold. This fold is called the "Schöberspitzen antiform" (Figs. 1b, 2). According to Rosenberg and Schneider (2008) and Töchterle et al. (2011), this fold developed at the western end of the SEMP fault (Fig. 1), accommodating its sinistral strike-slip motion. The entire western Tauern Window plunges westwards, as indicated by the descent of the top of the Venediger duplex (Fig. 2).

The Brenner normal fault

The Brenner normal fault forms the western boundary of the Tauern Window (Fig. 1b; e.g,. Schmidegg 1953, 1954; Behrmann 1988; Selverstone 1988; Axen et al. 1995; Fügenschuh et al. 1997, 2012; Rosenberg and Garcia 2011, 2012). It consists of a viscous part (Brenner mylonites) between Steinach and Sterzing (Behrmann 1988; Selverstone 1988; Fig. 1b) and a brittle part that overprints the Brenner mylonites (e.g., Prey 1989; Axen et al. 1995; Fügenschuh et al. 1997, 2012) and continues north to Innsbruck (Silltal fault; Schmidegg 1953, 1954; Fig. 1b). We only focus on the viscous Brenner normal fault in this work, because it was mainly involved in the process of exhumation of the western Tauern Window during the Miocene (Schmid et al. 2013 and references therein). The thickness of the mylonitic shear zone ranges from 0.4 km (Behrmann 1988) to 1.5 km (Wolff et al. 2021 and references therein). It dips gently to the west with an average angle of 20° (Axen et al. 1995). Its northern and southern continuation, however, is a matter of

debate: Fügenschuh et al. (1997, 2012) and Töchterle et al. (2011) propose that the viscous Brenner normal fault acted together with the Tauern northern boundary fault (TNBF) as a down-faulting envelope surrounding the western Tauern Window (Fig. 1b). According to their model, the brittle Silltal fault proceeding north to Innsbruck developed in a later stage. In contrast, Rosenberg and Garcia (2011, 2012) and Rosenberg et al. (2018) regard the brittle Silltal fault as the brittle, upper crustal part of the Brenner normal fault, which was tilted northwards during updoming of the core of the western Tauern Window. Rosenberg et al. (2018) additionally suggest different mylonites generation sets in the Brenner Pass area, where exhumation was highest. Both models are based on zircon fission-track data, which date to the Miocene in the Penninic and Subpenninic units of the western Tauern Window, but to the Paleocene-Eocene in the adjacent Austroalpine units north of the TNBF (see compilation of Bertrand et al. 2017). The spatial resolution of the available data is, of course, relatively coarse. No closely sampled profile is available. Rosenberg and Garcia (2011, 2012) and Rosenberg et al. (2018) propose a gradual northward increase in age, attributed to the progressive updoming of the western Tauern Window during the Miocene. In contrast, Fügenschuh et al. (1997, 2012) assume a discrete zircon fission-track age jump across the TNBF, linked to the eastward continuation of normal faulting kinematics associated with the viscous Brenner normal fault. For its northern extension, we follow the model of Fügenschuh et al. (1997, 2012). This is supported by the observation that, northwest of Mayrhofen (Fig. 1b), the zircon fission-track sample locations from the Austroalpine and Penninic nappes across the TNBF are quite close (approximately 6 km), yet exhibit a significant age difference of approximately 35–45 Ma over this short distance (compilation of Bertrand et al. 2017). There is thus little room between the two data points for a gradual transition similar to the one observed in the core of the Tauern Window. However, field evidence of the TNBF was only found in the westernmost Tauern Window (Fügenschuh et al. 1997, 2012; Töchterle et al. 2011; Schmid et al. 2013), whilst its eastern extension remains unclear. Nevertheless, we would like to emphasise that both aforementioned models of the northern continuation of the Brenner normal fault are sound, and it is not the purpose of this study to rekindle this debate. For that, we refer here to the works of Fügenschuh et al. (1997, 2012), Rosenberg and Garcia (2011, 2012) and Rosenberg et al. (2018).

The southern continuation of the Brenner normal fault is difficult to define, too. There are three possibilities:

(1) Enveloping also occurred in the south suggesting that the Brenner normal fault transitions towards southeast into a viscous precursor of the Sterzing Mauls fault (Fig. 1b; Fügenschuh et al. 1997, 2012; see also Bistacchi et al. 2010) and, further east, into the Defereggen Antholz Vals (DAV) fault. North of the DAV fault, zircon fission-track data are Miocene in contrast to older zircon fission-track data south of the DAV fault (Eocene to Mesozoic ages; Bertrand et al. 2017; Klotz et al. 2019), indicating that relative north-side up movement took place along the DAV fault in the Miocene. By contrast, zircon fission-track ages across the Sterzing Mauls fault are mainly Miocene on both sides, suggesting that no important relative uplift happened on this fault in the Miocene.
(2) The Brenner normal fault merges into the Jaufen fault (e.g., Fig. 1b; Rosenberg and Garcia 2011, 2012; Rosenberg et al. 2018). This would be in line with zircon fission-track data of Paleocene-Eocene age indicating earlier cooling north (hanging-wall) of the Jaufen fault (Pomella et al. 2012; Bertrand et al. 2017) and Miocene zircon fission-track data in the footwall. However, according to Fügenschuh et al. (2012) and Luth et al. (2013), there is no evidence that the mylonites along the Jaufen fault genetically correlate with the mylonites of the viscous Brenner normal fault.
(3) The Brenner normal fault dies out both to the north and south; however, structural evidence is missing (see Rosenberg et al. 2018 for discussion).

We therefore consider possibilities (1) and (2) as the most realistic in our model.

Database and methods

Map compilation and structural data analysis

Before constructing our 3-D model of the western Tauern Window, we first created a compiled and simplified tectonic map of the major tectonic units and faults of the western Tauern Window (Fig. 1b). We compiled maps of AA.VV. (1930a, b, 1960a, b), Amt für Geologie und Baustoffprüfung (2007), Brandner et al. (2008c), Rockenschaub and Nowotny (2009), Rockenschaub et al. (2011), Moser (2011, 2012), Kreuss (2013, 2018), Schmid et al. (2013), Autonome Provinz Bozen–Südtirol (2014), Moser and Pavlik (2014) and GeoSphere Austria (2017). The vectorised data of the final tectonic map were inserted into MOVE™ and projected onto a 25 m resolution digital terrain model (DTM; European Environment Agency 2016).

In the next step, we integrated structural data, including fold axes and foliation planes (data of Schneider 2015, Brandner et al. 2008c and from own fieldwork—Table A1 in the Supplementary Information; note: fold axes not reported on the map of Brandner et al. (2008c), but the dataset used in this study was kindly provided by the Brenner Base Tunnel

project company (BBT-SE)). We make use of foliation plane measurements for constructing nappe surfaces for the 3-D modelling (Figs. 3a, 4a; see section "3-D modelling"). Local fold axes (Fig. 5; see also Table A1 in the Supplementary Information) were analysed to set up the 3-D model and were used as a proxy to quantify the lateral changes of both the azimuth and the plunge of the large-scale fold axes of the nappes of the western Tauern Window (Fig. 4c). The plunges of the fold axes were also used to verify the projection of the tops of the nappes above the present-day topographic surface and compare it with the cross-section of Schmid et al. (2013; Fig. 2b). We analysed fold axes from the Ahorn nappe and Tux nappe (panels 1, 3 and 4 in Fig. 5) separately from those of the Zillertal nappe (panels 5–7 in Fig. 5) and the Schöberspitzen antiform (panel 2 in Fig. 5) to identify possible differences in geometry and orientation between these antiforms. Equal-area lower-hemisphere stereographic projections and Kamp contours of the fold axes were created by using the software package Stereonet 11 (Allmendinger et al. 2012; Allmendinger 2022).

3-D modelling

Major tectonic basement units

Our 3-D model comprises the Penninic and Subpenninic nappe systems between ca. 15 km a.s.l. and 5 km b.s.l. We modelled the bases of four major tectonic nappes: the Tux nappe, the Zillertal nappe, the Subpenninic hanging-wall nappes and the Penninic nappe system. We started with the base of the structurally highest nappe (Penninic nappe system), because it continuously envelopes the Subpenninic nappe system below and, thus, best reflects the general structure of the western Tauern Window. In the following, we describe the workflow to construct the base of the Penninic nappe system in 3-D, step by step. Each step is visualised in Fig. 6, using sketches (see Fig. 4 for two real modelling examples). The other nappe bases were modelled in the same way; step numbering according to Fig. 6:

(1a and b) In a first step, we digitised the base of the Penninic nappe system as polylines in both the Brenner Base Tunnel section (Fig. 2a; Töchterle et al. 2007) and the cross-section of Schmid et al. (2013; Fig. 2b), close to the TRANSALP seismic section (Fig. 1b). We then interpolated a preliminary surface between both polylines using a spline curve tool (*Create Surface from Lines* in the *Surface* toolbox). Separately, we analysed fold axes as described above (Fig. 5).

(2a) We constructed two WSW–ENE along-strike cross-sections, following the hinges of the preliminary surfaces of the Tux nappe and the Zillertal nappe, respectively. In these cross-sections, we plotted the intersection of the preliminary surface (*mesh intersection*) and modified it to match the projected surface outcrops of the base of the Penninic nappe system (*line intersection*) and the fold axes data analysis (see also Fig. 5c). We did this as a first approximation of the lateral change of the plunge of the fold hinges.

(2b) To model the base of the Penninic nappe system west of the Brenner Base Tunnel section, we used its trace in the Brenner Base Tunnel section and split it into three parts: Trace of the Schöberspitzen antiform, the Tux nappe and the Zillertal nappe. These polylines were used as input objects for the extrapolation (*Extrude Line to Surface* in the *Extend* toolbox). For the Tux and Zillertal nappe traces, we used the average azimuth and plunge values of the fold axes of the respective structure in this area (panel 4 and 7 of Fig. 5) as the projection direction. The average value of the plunge of the Schöberspitzen antiform, if projected onto the Brenner Base Tunnel cross-section (panel 2 in Fig. 5), however, does not match its actual position of the antiform in the cross-section. We therefore derive the plunge of the Schöberspitzen antiform by extrapolating a surface from their polylines, as mapped on the land surface, choosing plunge and plunge azimuth values so that the extrapolated surface intersects with the position of the Schöberspitzen antiform in the Brenner Base Tunnel section (270/25). Close to the Brenner normal fault, we constructed a new cross-section (red line west of the Brenner Base Tunnel section). The three newly constructed surfaces were then displayed as traces in this cross-section (*mesh intersection*). These traces of the Tux nappe and the Zillertal nappe were then used again to extrapolate (*Extrude Line to Surface* in the *Extend* toolbox), as previously described, but this time using the orientation of the Brenner normal fault as input value, which is 20°W on average (Axen et al. 1995). The reason for this is that we assume that during exhumation the footwall of the viscous Brenner normal fault was dragged parallel to the dip of this fault.

(3) The newly created surfaces were then adapted to fit the outcrop information on the land surface, i.e. the foliation strike and dip, and the lateral change in elevation of the fold hinges, which we obtained from step (2a). For this purpose, we constructed 15 additional cross-sections. In each cross-section, we projected the preliminary surface (*mesh intersection*), the base of the Penninic nappe system, as mapped on the land surface (*line intersection*) and—for the elevation of the fold hinges—the lines constructed in (2a; *line intersection*). Dip data of the foliation was used to correct the geometry of the folds. In each cross-section, we thus constructed the base of the Penninic nappe system (see also Fig. 4a).

(4) Finally, we interpolated a new surface of the base of the Penninic nappe system between the cross-sections, using again a spline curve tool (*Create Surface from Lines* in the *Surface* toolbox).

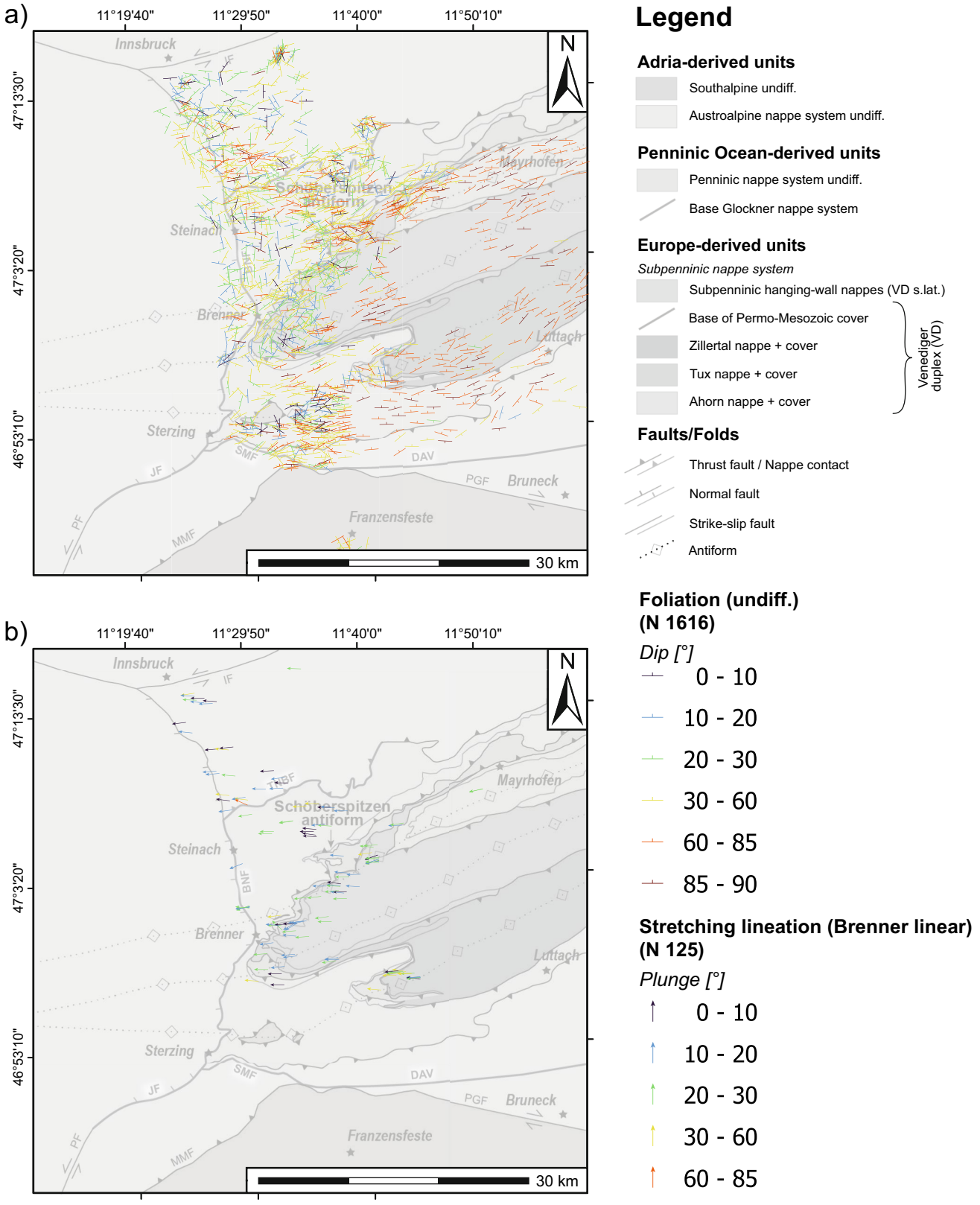

Fig. 3 **a** Compilation of foliation data (Brandner et al. 2008c; Schneider 2015; own data—A1), colour-coded according to dip [°]. Classification ranges are based on Schneider (2015). **b** Stretching lineations taken from Brandner et al. (2008c), colour-coded according to plunge. We use the same classification ranges as the foliation dip. Note: stretching lineations are not reported on the map of Brandner et al. (2008c), but the dataset used in this study was kindly provided by the Brenner Base Tunnel project company (BBT-SE)

Faults

In this paragraph, we focus on the viscous Brenner normal fault and its possible northern and southern continuations (bold red lines in Figs. 1b and 5). In our interpretation, this is the TNBF in the north, following Fügenschuh et al. (1997) and Töchterle et al. (2011). In the south, we modelled two options to analyse potential geometrical effects on the structure of the western Tauern Window: continuation into (1) the Sterzing Mauls fault (Fügenschuh et al. 1997, 2012) and DAV fault (derived from zircon fission-track data, Bertrand et al. 2017 and references therein), or (2) the Jaufen fault (Rosenberg and Garcia 2012, and derived from zircon fission-track data, Bertrand et al. 2017 and references therein).

For fault surface modelling, we used extrapolating methods (*Extrude Line to Surface* in the *Extend* toolbox), as we did in modelling step (3b). We used the polylines of the outcropping faults on our tectonic map as input objects and extruded them using the average dip direction and dip of the respective fault (see Table 1). Between the Sterzing Mauls fault and the eastern end of the DAV fault (on our map), we interpolated the along-strike change in dip (Fig. 5 and Table 1) by dividing the total change by the number of cross-sections. For this purpose, we drew a line in each relevant cross-section, which presumably predicts the local dip of the fault. At the end, we interpolated these lines to a new surface (*Create Surface from Lines* in the *Surface* toolbox), in the same way as we did in modelling step (4).

Finally, we intersected, interpolated and merged the isolated faults, which resulted in two Brenner normal fault models: (1) TNBF—Brenner normal fault—Jaufen fault, and (2) TNBF—Brenner normal fault—Sterzing Mauls fault—DAV fault.

Nappe geometry analysis and new cross-sections

Once the base of the Penninic nappe system was modelled, we analysed its structure (using *Surface Geometry* and *Contour Map*). This was only done with this particular surface, because, as mentioned above, it reflects best the structure of the western Tauern Window. The following surface properties were chosen: elevation, cylindricity, dip and dip azimuth.

In the end, we constructed new cross-sections throughout the entire model, including the two end-member models of the viscous Brenner normal fault: Five NNW-SSE striking, planar cross-sections (S1–S5) and two planar cross-sections, which trace the fold axes of the Tux nappe and the Zillertal nappe (W-ENE; S6–S7). Cross-section traces are shown in Fig. 1b. For better visualisation, we only illustrate the Penninic nappe system, the Subpenninic hanging-wall nappes, the Venediger duplex, and the faults above the present surface. From this, we obtained a good representation of the lateral changes of the large-scale structure of the western Tauern Window.

All modelled surfaces, the attribute analysis of surfaces of the Penninic nappe system base (colour-coded), and the new cross-sections can be viewed in the 3-D PDF via the link in the Data availability statement or in the Supplementary Information (Figs. A8 and A9).

Results

The overall folded structure of the western Tauern Window is best visualised by reference to the attribute analysis of the base of the Penninic nappe system surface (Fig. 7). Since the underlying Subpenninic nappe system follows this structure (see Figs. A8 and A9 in the Supplementary Information), we refer to the base of the Penninic nappe system surface to describe the western Tauern Window in general in the following.

Elevation and fold axis analyses reveal that the western Tauern Window plunges between 13° and 19° to the west (Figs. 5, 7a). However, there is a difference between the Tux antiform and the Zillertal antiform. Whilst the Tux antiform plunges almost continuously to the west-southwest, the plunge of the Zillertal antiform in the same direction is interrupted and becomes nearly horizontal over a distance of ca. 10 km, forming a kind of 'plateau' (white box in Figs. 7a and 8c; see also stereonet plot 6 in Fig. 5). In addition, deviation from a cylindrical shape (Fig. 7b; where green colour expresses perfect cylindricity) is strong in this area and becomes greater towards the west. In contrast, the Tux antiform is nearly cylindrical. Only parts of its southern limb and the easternmost part of its northern limb deviate from a perfectly cylindrical fold. Dip (Fig. 7c) and dip azimuth (Fig. 7d) analyses show that the southern limb of the Zillertal antiform's southern limb changes its dip abruptly from south-southeast (in the east) to north (in the west). Where its southern limb is steepest (90°; at the position, where the switch from an upright fold to an overturned fold happens), the trend of the fold axis turns to the southwest over a short distance, which is also accompanied by a strong deviation from cylindricity (just east of the white boxes in Fig. 7). West of this area, the southern limb of the Zillertal antiform is overturned. Generally speaking, all attribute colour maps show that, starting in the east, the fold axis of the Zillertal antiform trends first west-southwest, then west, then southwest (as mentioned before) and then again west. The Schöberspitzen antiform axis trends west, and the Tux antiform plunges west-southwest (Fig. 7; see also Fig. 5).

The developing Schöberspitzen antiform, the steepening of the southern limb of the Ahorn and Tux antiform, the overturning of the Zillertal antiform and the plunge of the entire western Tauern Window, all in western direction, are

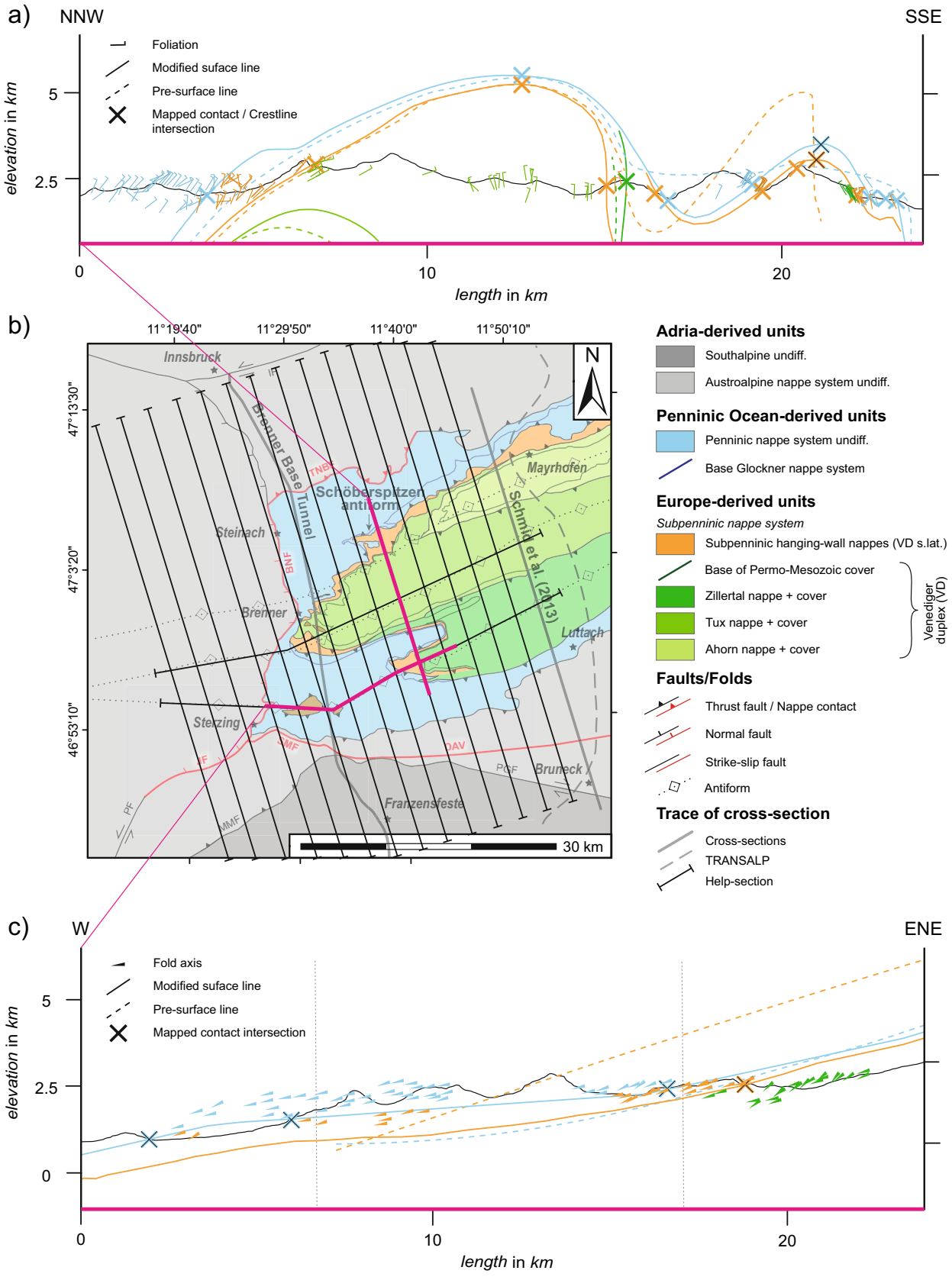
a)
NNW
SSE
Foliation
Modified suface line
Pre-surface line
Mapped contact / Crestline intersection
elevation in km
5
2.5
0
10
20
length in km
b)
11°19'40"
11°29'50"
11°40'0"
11°50'10"
47°13'30"
47°3'20"
46°53'10"
N
Innsbruck
Brenner Base Tunnel
TNBT
Schöberspitzen antiform
Mayrhofen
Steinach
BNF
Brenner
Schmid et al. (2013)
Luttach
Steinzing
UME
DAV
PGF
Brunneck
Franzensfeste
PF
MMF
30 km
Adria-derived units
Southalpine undiff.
Austroalpine nappe system undiff.
Penninic Ocean-derived units
Penninic nappe system undiff.
Base Glockner nappe system
Europe-derived units
Subpenninic nappe system
Subpenninic hanging-wall nappes (VD s.lat.)
Base of Permo-Mesozoic cover
Zillertal nappe + cover
Tux nappe + cover
Ahorn nappe + cover
Venediger duplex (VD)
Faults/Folds
Thrust fault / Nappe contact
Normal fault
Strike-slip fault
Antiform
Trace of cross-section
Cross-sections
TRANSALP
Help-section
c)
W
ENE
Fold axis
Modified suface line
Pre-surface line
Mapped contact intersection
elevation in km
5
2.5
0
10
20
length in km

◂**Fig. 4** 3-D modelling examples (**a**, **c**) of two cross-sections in the map (**b**). The dashed lines in a and c represent the intersected pre-surfaces constructed between the cross-sections of Töchterle et al. (2007) and Schmid et al. (2013). These polylines were modified according to foliations (**a**) and fold axes (**c**), as well as the outcrops of the base of the nappes along the topography (*line intersection*). W-E cross-sections were modified before the NNW-SSE cross-sections were constructed to obtain the height of the fold hinges of the Tux antiform and the Zillertal antiform (crosses in the fold hinges of a). Note: the fold axis dataset used in this study was kindly provided to the authors by the Brenner Base Tunnel project company (BBT-SE)

demonstrated in the cross-sections in Fig. 8. It can also be observed that the Tuxer and Zillertal antiform tighten and become south-vergent westwards, in contrast to the Ahorn antiform, which opens and would seem to become box-shape-like in the same direction (Fig. 8a).

Regarding the Brenner normal fault and the thickness of the Penninic nappe system in its footwall, we found that the Penninic nappe system in the footwall of the Brenner normal fault is thinner above the Tux nappe than above the Zillertal nappe. The maximum distance between top of the Tux nappe and the Brenner normal fault (i.e. the thickness of the Penninic nappe system) reaches ca. 3 km (Fig. 8b). On the contrary, where the Zillertal nappe reaches its 'plateau', the thickness of the Penninic nappe system is between ca. 4 and 6 km (Fig. 8c). At a point directly west of the apex of the Zillertal nappe, the known trace of the Brenner normal fault ends.

The two possible southern continuations of the Brenner normal fault are shown in Fig. 8a (see also Figs. A8 and A9 in the Supplementary Information). Regarding the completely-enveloping variant (TNBF—Brenner normal fault—Sterzing Mauls fault—DAV fault), it appears that the envelope is quite similar to the form of the Zillertal nappe antiform. Regarding the second variant, in which the Brenner normal fault merges with the Jaufen fault, it can be seen in cross-section view (Fig. 8a; see also Figs. A8 and A9 in the Supplementary Information) that the distance between the top of the hinge of the Zillertal antiform and the Brenner and Jaufen faults, increases southwards (apparent northern dip of the Jaufen fault and the southern part of the Brenner normal fault; Fig. 8a; see also Figs. A8 and A9 in the Supplementary Information).

Discussion

Model uncertainties

Our 3-D model is based on the cross-sections of Töchterle et al. (2007) and Schmid et al. (2013). The upper ca. 2 km of the cross-section of Töchterle et al. (2007) are very well constrained, based on data from the Brenner Base Tunnel exploration. The area below is more speculative and is based mainly on field observations and projections from further east. The cross-section of Schmid et al. (2013) is based mainly on field observations, information from the TRANSALP interpretation (TRANSALP Working Group 2002; Lüschen et al. 2004, 2006; Lammerer et al. 2008) and projections from the surrounding areas—especially above the topography. The position of the fold hinge of the Tux antiform is consistent with our fold axes analysis. We could not verify the position of the fold hinge of the Zillertal antiform, because we do not have data from fold axes east of box/panel 5 (Fig. 5). If only the data of box/panel 5 (Fig. 5) were used for projection, the top of the Zillertal antiform in the cross-section of Schmid et al. (2013) would be constructed too high. However, the outcrop of the Zillertal core east of box/panel 5 (Fig. 5) widens, which may indicate that its plunge steepens here.

In cross-section 3 of Schmid et al. (2013), the nappe contacts between the three antiforms are folded. However, we did not take these folds into account in our 3-D model. We simplified the complex-folded structure of the western Tauern Window, as we want to represent its overall, larger-scale structure.

Foliation data east of the map of Töchterle et al. (2007) were taken from Schneider (2015). However, the classification ranges of these dips are quite large. For our modelling, we therefore only use the map and the legend information from her dissertation (Schneider 2015), which is why these values were taken as trends in the modelling.

The orientation of the Brenner normal fault is based on the derived average value of the dip of this fault from Axen et al. (1995), based on their rolling hinge model. Field data show a shallower dip between 15° (Fügenschuh et al. 1997) and 17° (Axen et al. 1995). We tried to apply these shallower values in the extrapolation, which results in a subparallelism to the dip of the Tux antiform (plunge of the Tux antiform between 13°–19° in our model). The average value of Axen et al. (1995) therefore serves as a maximum value.

A shallower dip of the Brenner normal fault also correlates with plunges of stretching lineations, which are associated with the viscous Brenner normal fault (Fig. 3b). Their plunges do not change eastward, which indicates that the viscous Brenner normal fault does not flatten towards the east, at least not in the area of the map made by Brandner et al. (2008c). However, we cannot exclude that the Brenner normal fault becomes shallower in the eastern part of our modelling area.

Modelling of the base of the Penninic nappe system results in apparent en-échelon folds superimposed on the Schöberspitzen antiform. These are modelling artefacts that resulted from surface interpolation.

The intersection of our modeled nappe bases with the DTM does not always perfectly match the mapped outcrops.

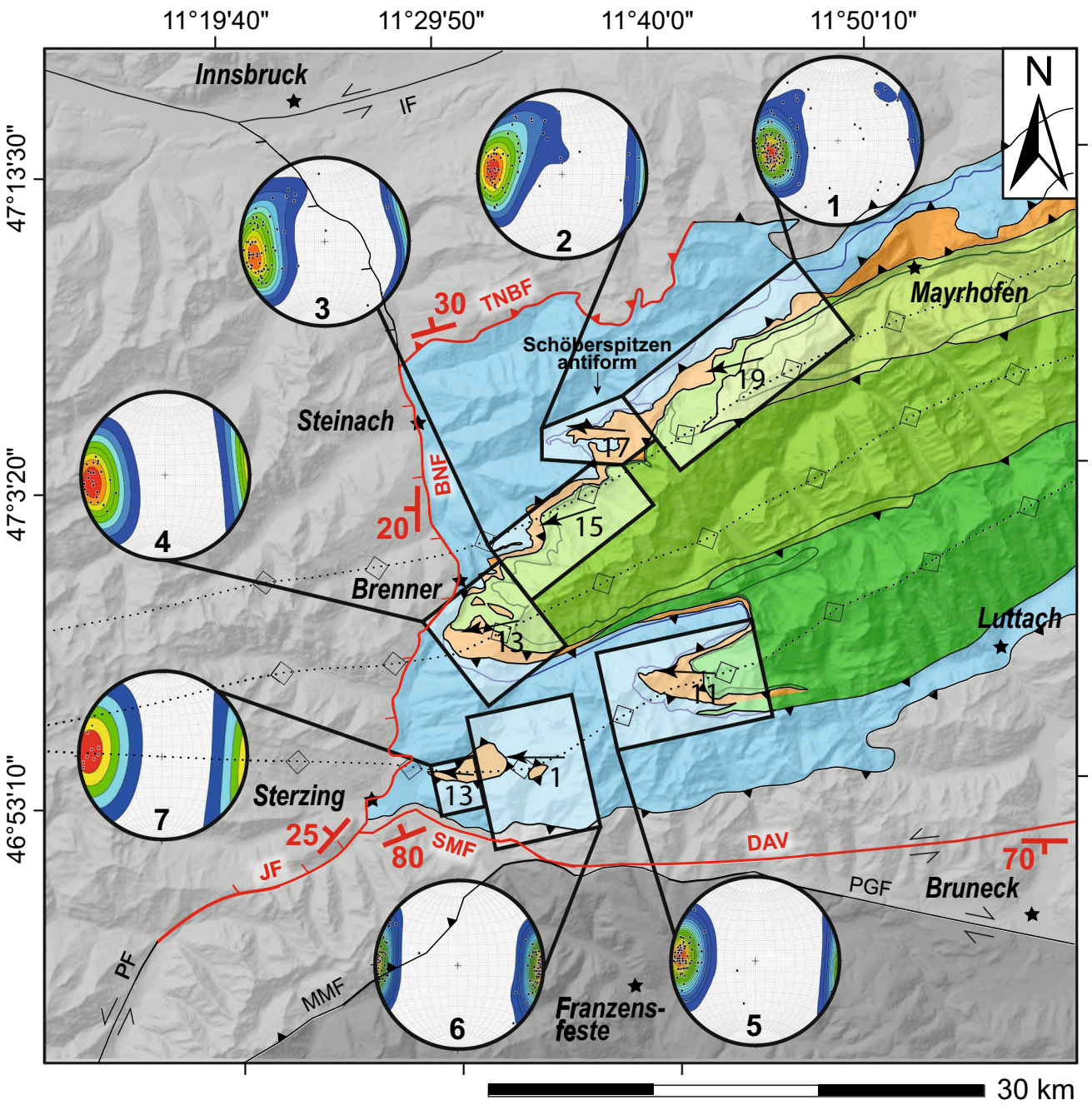

Fig. 5 Equal-area lower-hemisphere stereographic projections and Kamp contours of fold axes of different areas (panels 1–7). Data taken from Brandner et al. (2008c), combined with the first author's field data (Table A1 in the Supplementary Information; see Figs. A1–A7 in the Supplementary Information for closer views of the stereographic plots; note: fold axes not reported on the map of Brandner et al. (2008c), but the dataset used in this study was kindly provided by the Brenner Base Tunnel project company (BBT-SE)). The arrow and the corresponding numbers in the boxes represent the mean azimuth and plunge of the fold axes of the area of this box. Average dip direction and dip is also illustrated for each fault that is relevant for the model (bold red symbols). References for these data are given in section "Faults". Fault abbreviations: *BNF* Brenner normal fault, *DAV* Defereggen Antholz Vals fault, *IF* Inntal fault, *JF* Jaufen fault, *MMF* Meran Mauls fault, *PGF* Pustertal Gailtal fault, *PF* Passeier fault, *SMF* Sterzing Mauls fault, *TNBF* Tauern northern boundary fault

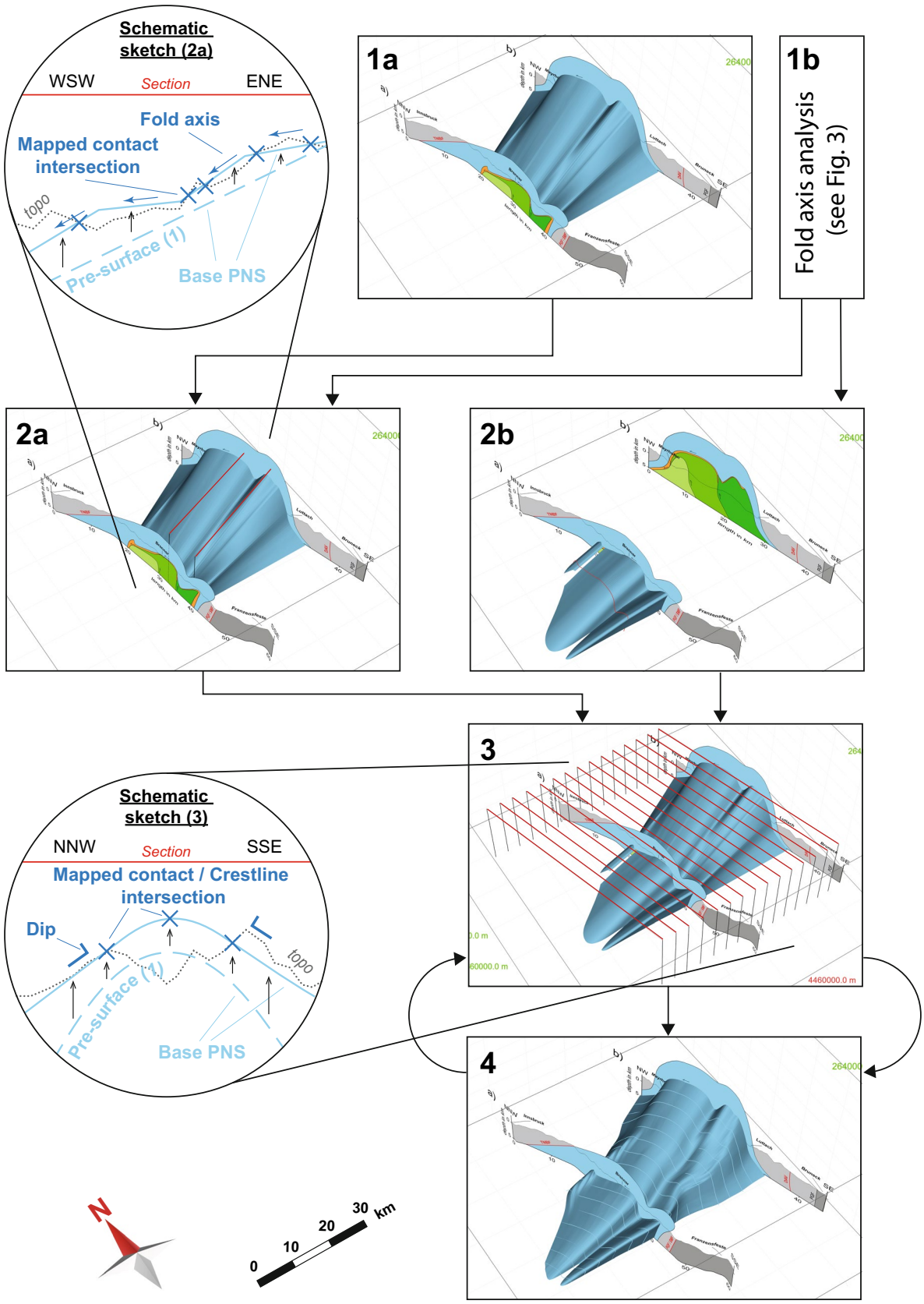

Fig. 6 3-D modelling workflow, using interpolating (1, 2a, 3 and 4) and extrapolating (2b) methods. For closer view of the two profiles, we refer to Fig. 2. For further explanation, see text

Table 1 Average values of dip direction and dip, and the related references that were used for fault surface modelling (see also Fig. 5)

Fault	Ø Dip dir./Dip	References
Brenner normal fault (viscous)	270/20	Axen et al. (1995)
DAV fault	180/70	Mancktelow et al. (2001)
Jaufen fault	310/25	Luth et al. (2013), Pomella et al. (2016), Klotz et al. (2019)
Sterzing Mauls fault	334/80	Töchterle et al. (2007), Klotz et al. (2019)
TNBF	345/30	Töchterle et al. (2011)

Areas where the intersection of the modeled surface with the DTM deviates slightly include the Schöberspitzen area, the western intersection of the Ahorn and Zillertal nappes, and the small window east of Sterzing (Fig. 1b). However, this is unavoidable at our model scale. For visualisation of the deviations, we refer to the 3-D PDF (see Data availability statement or Supplementary Information, Fig. A9) and Fig. A10 in the Supplementary Information.

In our model, we projected the bases of the nappes in western direction, based on the westernmost available data. In fact, we do not know, whether the western Tauern Window continues plunging in western direction, or if the nappes deflect west of the tip of the Dolomites indenter.

From the static 3-D model of the western Tauern Window to its Miocene deformation history

The Tux and Zillertal antiforms are similar in that they tighten and become south-vergent along-strike in a westerly direction and thus, towards the tip of the Dolomites indenter (c.f. Figs. 7c, d, 8; Töchterle et al. 2007; Brandner et al. 2008a), which has a triangular shape in map view (Fig. 1). In contrast, the Ahorn antiform opens in a westerly direction and it seems to become box-shaped, with no marked vergence (Fig. 8). However, we observe that the along-strike development of the bulge on its northern limb coincides with the appearance of the Schöberspitzen antiform. We therefore assume that this northern bulge formed in the course of the development of the Schöberspitzen antiform. If we additionally consider the deeper structure published in Reiter et al. (2018), the Ahorn antiform does show south-vergence, similar to the Tux and Zillertal antiforms.

The nappes in the vicinity of the TRANSALP seismic section are upright folds (c.f. Figs. 7c, d, 8; Lüschen et al. 2004, 2006; Lammerer et al. 2008; Schmid et al. 2013; Rosenberg et al. 2018). The stronger deformation of the Zillertal antiform (smaller interlimb angle, non-cylindrical fold; Figs. 2, 7, 8) compared to the Tux antiform is most likely due to the fact that it is the southernmost antiform and thus closest to the Dolomites indenter. Whilst indentation only verticalized the southern limb of the Tux antiform, the Zillertal antiform became overturned. The transition point from an upright fold in the east to an overturned fold in the west is not located directly in front of the indenter's present-day tip (on map view), but it is approximately 5 km eastwards. This discrepancy may be due to the reorganisation of the middle and lower crust of the Dolomites indenter: interpretation of seismic tomography of this area indicates thickening of the lower crust in the vicinity of the TRANSALP seismic section (McPhee and Handy 2024; Handy 2025). McPhee and Handy (2024) interpret this as detached middle and lower crust of the Dolomites indenter. This detachment occurred along a north-dipping ductile shear zone within the intermediate crust in which south-directed thrusts of the Dolomites indenter (e.g., Valsugana thrust, Belluno thrust) root (see also e.g., Schönborn 1999; Verwater et al. 2021; Eizenhöfer et al. 2023). In contrast, thickening of the lower crust is not noticeable near the Brenner Base Tunnel (McPhee and Handy 2024 and references therein). We conclude that in the vicinity of the Brenner Base Tunnel, the upper and lower crust of the Dolomites indenter were indented together without being detached, whereas below the TRANSALP section, the middle and lower crust of the Dolomites indenter seems to be detached and this part wedges below the Subpenninic nappe system (Fig. 9). We hypothesise that the gradually-increasing detachment of the middle and lower crust of the Dolomites indenter from west to east is expressed in the structure of the upper crust above (i.e. the western Tauern Window), by the transition from south-vergent (Ahorn and Tux antiforms) and overturned folds (Zillertal antiform) in the west to upright folds in the east of our study area.

Consider a perfectly cylindrical fold in a viscous environment with no particular vergence direction. If an indenter pushes normal to the fold axis, (depending on the indenter's shape) the fold would become tighter. Over time, the limb facing the indenter would progressively steepen and the fold would finally overturn. However, if at one point during indentation, the middle and lower crust of the indenter detached and underthrusted the fold ahead, folding would cease and the entire structure would be pushed upwards instead. We hypothesise that this is expressed by the curved trend of the Zillertal antiform fold axis and the western plunge of the entire western Tauern Window: In the west, steady indentation of the entire Dolomites indenter's crust caused south-vergence (Ahorn and Tux antiforms) and overturning folds (Zillertal antiform), respectively (Fig. 9

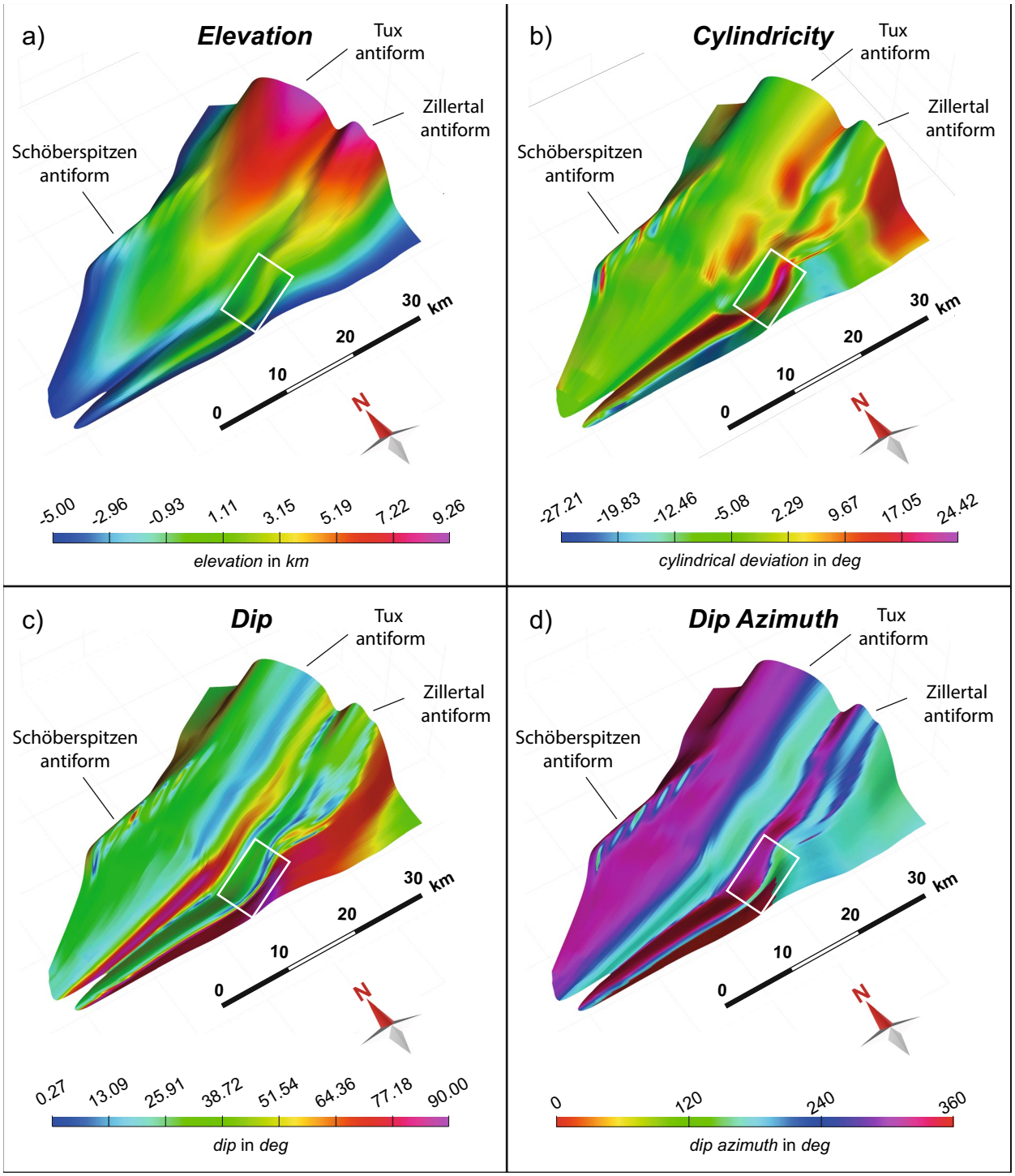

Fig. 7 Colour maps of different structural properties (attributes) of the base of the Penninic nappe system: **a** elevation, **b** cylindricity (i.e., mismatch of a normal to a surface triangle with respect to a normal to the average cylindrical vector of the surface (in this case 254.6/15.4); positive values mean tighter, negative values mean wider than the cylindrical surface), **c** dip and **d** dip azimuth. The white box shows the area in which the western plunge of the Zillertal antiform is interrupted. For details of the analyses, see text

"west"). In the east, the middle and lower crust of the Dolomites indenter detached and indented, at least faster than the upper crust, underthrusting, and pushing-up the nappe stack of the western Tauern Window (Fig. 9 "east"). The westward plunge of the entire western Tauern Window would then be a consequence of this underthrusting, which, depending

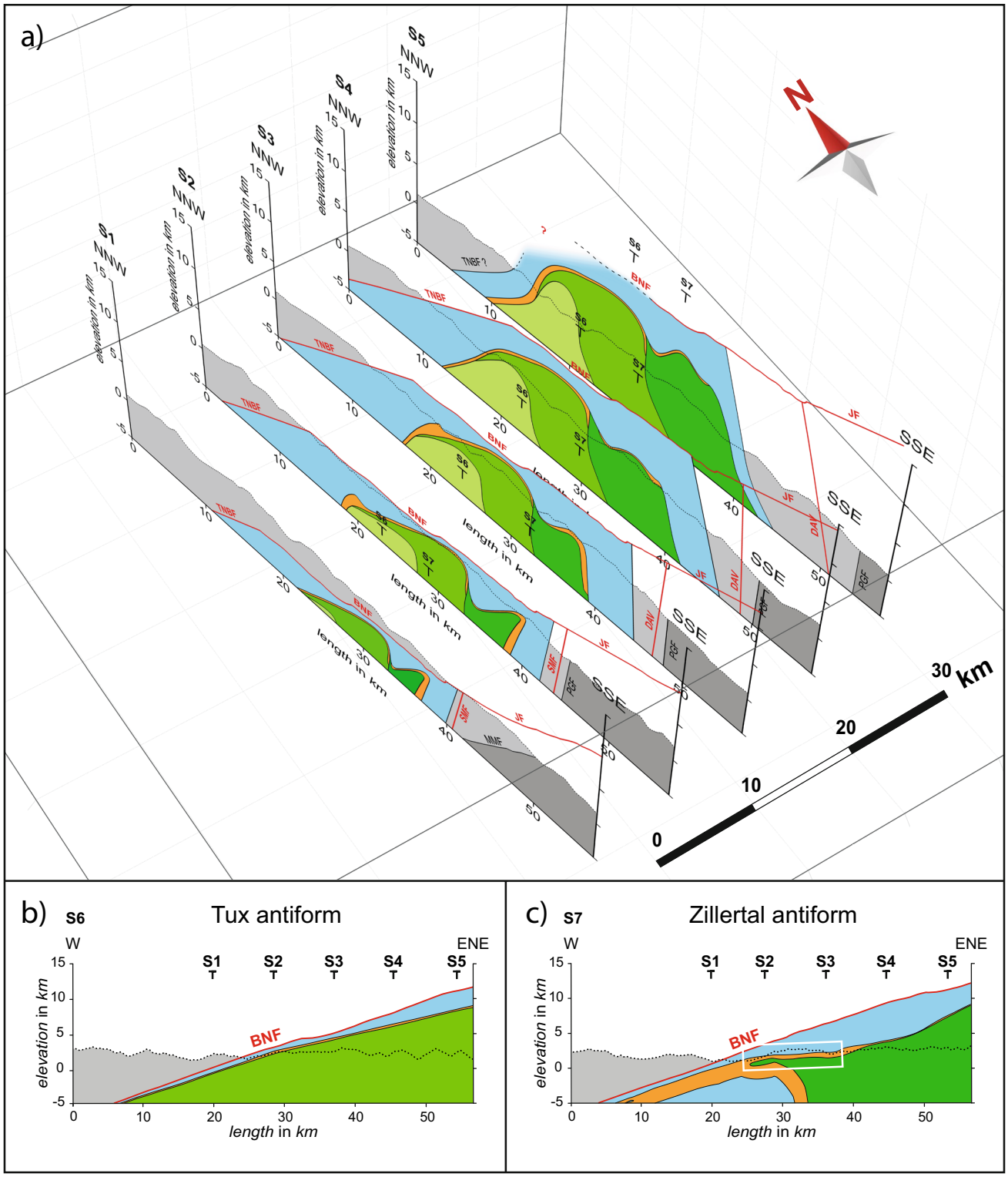

Fig. 8 New cross-sections through the western Tauern Window, based on the 3-D model. **a** NNW-SSE cross-sections (S1–S5), **b**, **c** W-ENE cross-section (S6–S7) along the traces of the fold axes. The traces of the cross-sections and the legend are shown in Fig. 1b. Cross-sections S1–S5 can be found in the Supplementary Information on a larger scale (Figs. A8 and A9). The white box shows the area in which the western plunge of the Zillertal antiform is interrupted (see also Fig. 7). Fault abbreviations: *BNF* Brenner normal fault, *DAV* Defereggen Antholz Vals fault, *IF* Inntal fault, *JF* Jaufen fault, *SMF* Sterzing Mauls fault, *TNBF* Tauern northern boundary fault

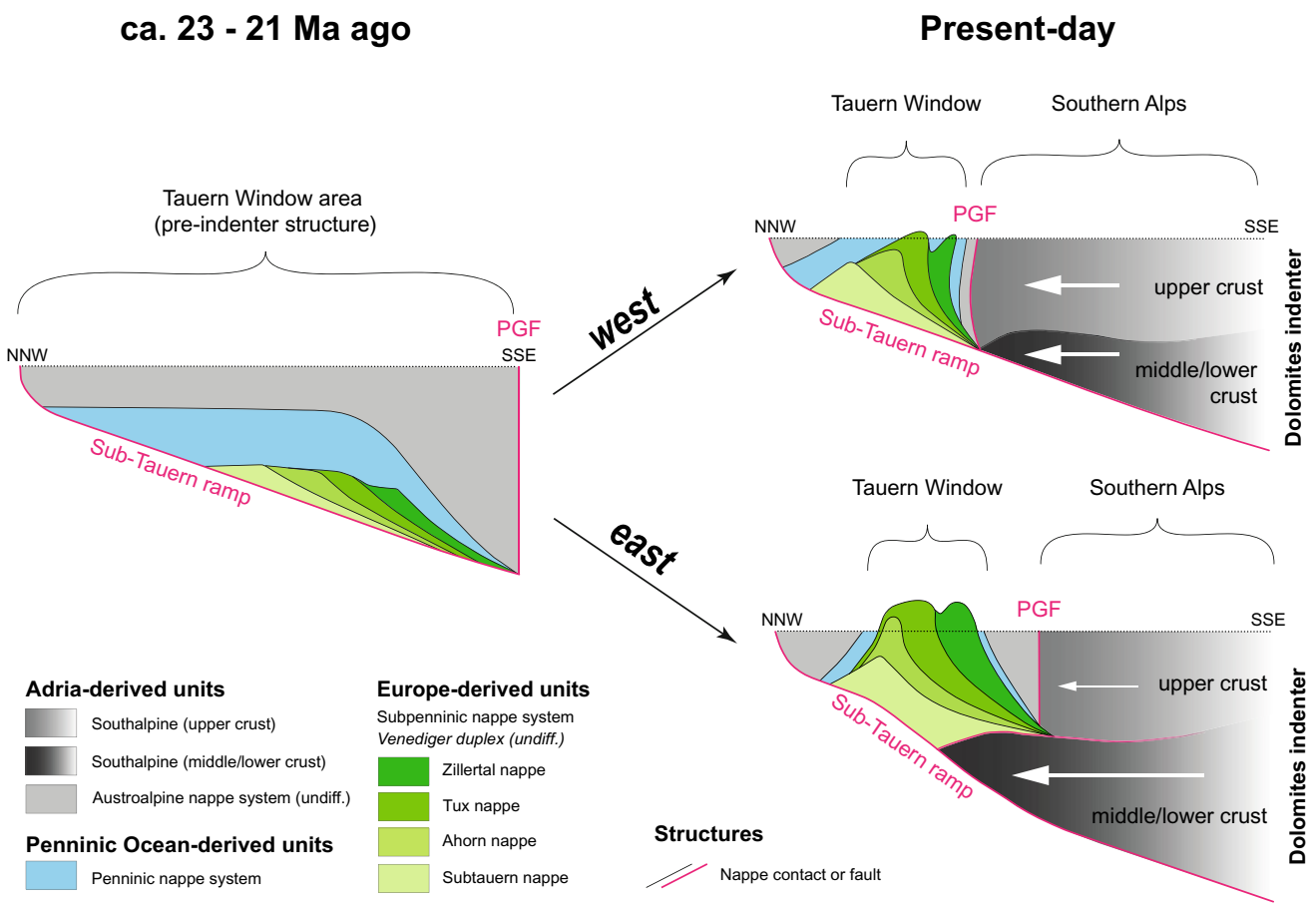

Fig. 9 Sketch of the differently-developed structures of the western Tauern Window. Left: pre-indenter structure (ca. 23 Ma ago; modified after Rudmann et al. 2025). Right: today's structure of the nappe stack of the western Tauern Window in the west (top right; based on Reiter et al. 2018) and east (bottom right; based on McPhee and Handy 2024) of our modelling area. For more details, see text. Note: While the areas of the nappes of the pe-indenter structure and the present-day structure in the west are balanced (see restoration of Rudmann et al. 2025), the areas of the nappes in the east appear larger in part (e.g., Subtauern nappe). However, this cross-section is a compilation of our model (upper crust; based on Schmid et al. 2013 in the east) and that of McPhee and Handy (2024) and references therein (middle and lower crust). Therefore, the surface areas of the nappes in the latter section have to be viewed with caution. *PGF* Pustertal-Gailtal fault

on its timing, either favoured the formation of the viscous Brenner normal fault, or steepened it (i.e. from an originally lower dip). From this thought experiment, we can also deduce that the upright folds in the east and the steepening of the southern limb of the Tux antiform in the west represent progressive stages of deformation, through which the Zillertal antiform must have once passed. That means that during an earlier phase of indentation, the western segments of both the Tux and Zillertal antiforms likely exhibited similar geometries to those observed in the east of our study area. Then, at a later stage, during ongoing indentation of all crustal parts of the Dolomites indenter, the Zillertal antiform developed into a structure similar to that of the Tux antiform in the west (verticalisation of the southern limb), before it experienced maximum deformation directly in front of the Dolomites indenter and became overturned. Hence, the pre-indentation structure of the Venediger duplex might have been everywhere very similar in our study area (Rudmann et al. 2025; Fig. 9), possibly across the entire Tauern Window (see also Rosenberg and Berger 2009).

The plunge of the Tux antiform coincides with the dip of the viscous Brenner normal fault (e.g., Axen et al. 1995; Fügenschuh et al. 1997). In contrast, the plunge of the Zillertal antiform is interrupted over a distance of about 10 km, forming a kind of 'plateau' that deviates from the dip of the Brenner normal fault. This also affects the thickness of the Penninic nappe system in the footwall of the Brenner normal fault, which is thinner between the top of the Tux antiform and the Brenner normal fault than above the 'plateau' of the Zillertal antiform and the Brenner normal fault (see Fig. 8b, c). The cause of this 'plateau' could be primary, lateral unevenesses or bumps of the Zillertal antiform, whereby the increasing plunge of the fold axes towards the west could be also associated with the Zillertal nappe

being pushed-up by the protuded middle and lower crust of the Dolomites indenter. Ca. 10 km from the plateau, in along-strike west-southwestern direction, the known trace of the Brenner normal fault ends. This is where the two different southern continuations of the viscous Brenner normal fault have been proposed: Brenner normal fault—Sterzing Mauls fault (Fügenschuh et al. 1997, 2011)—DAV fault (derived from zircon fission-track data, Bertrand et al. 2017 and references therein) or Brenner normal fault—Jaufen fault (Rosenberg and Garcia 2011, 2012, and derived from zircon fission-track data, Bertrand et al. 2017 and references therein). Both scenarios result in the aforementioned greater distance between the Zillertal nappe 'plateau' and the viscous Brenner normal fault. Our model cannot provide any indication as to which Brenner normal fault scenario is correct. However, it is most likely that it is a combination of both scenarios. Zircon fission-track ages suggest top-to-SE thrusting on the Meran Mauls fault contemporaneously with uplift of the western Tauern Window (Pomella et al. 2012; Bertrand et al. 2017). This means that north-side up movement along the DAV fault did not continue along the Sterzing Mauls fault to the west, as proposed by Fügenschuh et al. (1997, 2012), but along the top-to-SE thrust along the Meran Mauls fault (e.g., Pomella et al. 2011, 2012; Luth et al. 2013; see also distribution of zircon fission-track data in Bertrand et al. 2017). Based on zircon fission-track data (Pomella et al. 2012; Bertrand et al. 2017) and structural field data (Viola et al. 2001; Luth et al. 2013; Pomella et al. 2022), the Austroalpine Meran-Mauls basement nappe stack was squeezed upwards (top-to-SE thrusting) between the NW-dipping Meran-Mauls fault at its base and the NW-dipping Jaufen fault at its top in the Miocene, due to its frontal position to the Dolomites indenter. In zircon fission-track contour maps (Pomella et al. 2012; Bertrand et al. 2017) this appears as a south-westward continuation of the young cooling ages characteristic for the Tauern Window.

According to Rosenberg and Schneider (2008) and Töchterle et al. (2011), the Schöberspitzen antiform accommodated sinistral motion at the western end of the SEMP fault. Our 3-D model supports this, because the plunge azimuth of the fold axis of the Schöberspitzen antiform (270°) is at an acute angle of approximately 20° to the west-southwest strike of the SEMP fault. The plunge of the fold axis of the Schöberspitzen antiform is sub-parallel to parallel to the western dip of the Neoalpine nappe contacts, which in turn is sub-parallel to the dip of the viscous Brenner normal fault. The Schöberspitzen antiform may have formed before the western Tauern Window started to tilt westwards and thus it rotated to the west in the course of this process, or it developed synkinematically with the continuously-increasing westward plunge during Miocene times. This overlaps with the activity of the SEMP fault, which is assumed to be bracketed between 33 and 12 Ma (Rosenberg and Schneider 2008; Favaro et al. 2017 and references therein).

Summary and conclusions

Our static 3-D model of the western Tauern Window provides new, valuable insights into its Miocene deformation history:

1. Structure: The Tux and Zillertal antiforms were heterogeneously deformed during Miocene times. The Tux antiform is nearly cylindrical and plunges uniformly to the west-southwest. In contrast, the Zillertal antiform's fold axis is curved in map view and its plunge is interrupted over 10 km distance, forming a kind of 'plateau'.
2. The influence of the Dolomites indenter: The deformation patterns of the western Tauern Window antiforms are closely linked to their proximity to the tip of the Dolomites indenter (in map view) and heterogeneous, asymmetrical indentation as has been suggested in recent publications. The upper crustal deformation of the nappes of the Tauern Window can be explained with decreasing upper crustal shortening of the western Tauern Window towards the east whilst in the same direction increasing underthrusting of middle and lower crust of the Dolomites indenter occurred, which also caused the westward plunge of the western Tauern Window.
3. The viscous Brenner normal fault: The dip of the viscous Brenner normal fault aligns with the plunge of the Tux antiform, but not everywhere, with the variable plunge of the Zillertal antiform that includes a subhorizontal 'plateau'. This affects the thickness of the Penninic nappe system in the footwall of the Brenner normal fault. The lateral change in plunge of the Zillertal antiform could be caused by primary unevenesses (e.g., intrusive shape, paleo-relief, horst graben structures) of the Zillertal nappe itself. However, the increased plunge east of the 'plateau' could be also due to the up-push of the Zillertal nappe by the protruded middle and lower crust of the Dolomites indenter. This in turn either facilitated the formation of the viscous Brenner normal fault, or (if normal faulting had already begun when detachment occurred) steepened it.
4. Schöberspitzen antiform: The Schöberspitzen antiform accommodates sinistral motion at the western tip of the SEMP fault. The westward plunge of this antiform is similar to the plunge of the entire western Tauern Window. This suggests that the Schöberspitzen antiform developed pre- or synkinematically to the westward plunge of the western Tauern Window, which evolved during the Miocene. The activity of the SEMP fault in

the same time period reinforces their temporal connection.

Supplementary Information The online version contains supplementary material available at https://doi.org/10.1007/s00531-025-02528-9.

Acknowledgements We thank the editor-in-chief, Prof. Dr. Ulrich Riller, and the reviewers, Jonas Kley and Claudio Rosenberg, whose reviews and comments significantly improved the manuscript. This study greatly benefitted from the discussion with and the support from Mark Handy, Simon Hinterwirth, Peter McPhee and Hugo Ortner. We also thank the entire AlpArray community for the very enriching poster discussions. We are grateful to acknowledge funding from the German Science Foundation (TA 427/5-1, BR 3779/6-1, STI 298/11-1) within the Priority Programme SSP-2017 "Mountain Building Processes in Four Dimensions (MB-4D)". In addition, we acknowledge Petroleum Experts (Petex) for providing an academic version of Move™, licensed to the Martin Luther University Halle-Wittenberg, and the free use of the software Stereonet 11 (Allmendinger et al. 2012; Allmendinger 2022).

Funding Open Access funding enabled and organized by Projekt DEAL. This work was funded by the German Science Foundation (TA 427/5-1, BR 3779/6-1, STI 298/11-1) within the Priority Programme SSP-2017 "Mountain Building Processes in Four Dimensions (MB-4D).

Data availability The simplified tectonic map of the research area is based on AA.VV. (1930a, b, 1960a, b), Amt für Geologie und Baustoffprüfung (2007), Autonome Provinz Bozen–Südtirol (2014), Brandner et al. (2008c), Geosphere Austria (2017), Kreuss (2013, 2018), Moser (2011, 2012), Moser and Pavlik (2014), Rockenschaub and Nowotny (2009), Rockenschaub et al. (2011) and Schmid et al. (2013). For the cross-sections, we used information of Brandner et al. (2008a), Rosenberg and Garcia (2011), Schmid et al. (2013) and Töchterle et al. (2007). Digital terrain models (25 m resolution), used for the topographic profile, were taken from the European Environment Agency (2016). Structural data were taken from Brandner et al. (2008c) and Schneider (2015). Note: the structural dataset used in this study was kindly provided to the authors by the Brenner Base Tunnel project company (BBT-SE). The structural data of Julia Rudmann can be seen in the Table A1 in the Supplementary Information. The 3-D PDF of the model can be found under this link: https://doi.org/10.6084/m9.figshare.27110206.

Declarations

Conflict of interest The authors declare no competing financial or personal conflict of interest or a personal relationship that influenced the work presented in this paper.

References

AA VV (1930a) Carta Geologica della Tre Venezie, Foglio 1^{A}, Vetta d'Italia. Servizio Geologico d'Italia

AA VV (1930b) Carta Geologica della Tre Venezie, Foglio 4^{A}, Bressanone. Servizio Geologico d'Italia

AA VV (1960a) Carta Geologica d'Italia, Foglio 4, Merano. Servizio Geologico d'Italia

AA VV (1960b) Carta Geologica d'Italia, Foglio 4^{A}, Bressanone. Servizio Geologico d'Italia

Allmendinger RW (2022) Stereonet 11: software for plotting and analyzing orientation data. https://www.rickallmendinger.net/stereonet. Accessed 20 Feb 2024

Allmendinger RW, Cardozo N, Fisher D (2012) Structural geology algorithms: vectors and tensors in structural geology. Cambridge University Press, Cambridge

Amt für Geologie und Baustoffprüfung (2007) Geologische Übersicht von Südtirol und der angrenzenden Gebiete. Geologische Haupteinheiten, Hauptstörungen. http://geokatalog.buergernetz.bz.it/geokatalog/#!. Accessed 27 Nov 2023

Autonome Provinz Bozen–Südtirol (2014) Geobrowser maps. https://maps.civis.bz.it/. Accessed 12 March 2024

Axen GJ, Bartley JM, Selverstone J (1995) Structural expression of a rolling hinge in the footwall of the Brenner Line normal fault, eastern Alps. Tectonics 14(6):1380–1392

Behrmann JH (1988) Crustal-scale extension in a convergent orogen: the Sterzing-Steinach mylonite zone in the Eastern Alps. Geodinam Acta 2(2):63–73

Bertrand A, Rosenberg C, Rabaute A, Herman F, Fügenschuh B (2017) Exhumation mechanisms of the Tauern Window (Eastern Alps) inferred from apatite and zircon fission track thermochronology. Tectonics 36(2):207–228. https://doi.org/10.1002/2016tc004133

Bistacchi A, Massironi M, Dal Piaz GV, Dal Piaz G, Monopoli B, Schiavo A, Toffolon G (2008) 3D fold and fault reconstruction with an uncertainty model: an example from an Alpine tunnel case study. Comput Geosci 34(4):351–372. https://doi.org/10.1016/j.cageo.2007.04.002

Bistacchi A, Massironi M, Menegon L (2010) Three-dimensional characterization of a crustal-scale fault zone: the Pusteria and Sprechenstein fault system (Eastern Alps). J Struct Geol 32:2022–2041. https://doi.org/10.1016/j.jsg.2010.06.003

Brandner R, Reiter F, Töchterle A (2008a) Überblick zu den Ergebnissen der geologischen Vorerkundung für den Brenner-Basistunnel. Geo Alp 5:165–174

Brandner R, Reiter F, Töchterle A (2008b) Hochmetamorphe Keuperfazies („Aigerbach-Formation") und unterjurassische Kontinentalrandfazies („Kaserer-Formation"), zwei Schlüssellithologien bei der geologischen Prognose für den Brenner-Basistunnel. J Alpine Geol 49:14. https://doi.org/10.13140/RG.2.2.33416.21763

Brandner R, Töchterle A, Pomella H, Reiner F (2008c) Brenner Basistunnel, Geologische Karte 1:50.000. Institute of Geology, University of Innsbruck. https://doi.org/10.13140/RG.2.2.10994.71366

Dachs E (1986) High-pressure mineral assemblages and their breakdown-products in metasediments South of the Grossvenediger, Tauern Window, Austria. Schweizerische Mineralogische und Petrographische Mitteilungen, pp 145–161

Dachs E (1990) Geothermobarometry in metasediments of the southern Grossvenediger area (Tauern Window, Austria). J Metamorph Geol 8(2):217–230. https://doi.org/10.1111/j.1525-1314.1990.tb00467.x

Eizenhöfer PR, Glotzbach C, Kley J, Ehlers TA (2023) Thermokinematic evolution of the Eastern European Alps along the TRANSALP transect. Tectonics. https://doi.org/10.1029/2022TC007380

European Environment Agency (2016) EU-DEM (raster)—version 1.1, Apr. 2016. https://sdi.eea.europa.eu/catalogue/srv/api/records/3473589f-0854-4601-919e-2e7dd172ff50. Accessed 15 August 2023

Favaro S, Handy MR, Scharf A, Schuster R (2017) Changing patterns of exhumation and denudation in front of an advancing crustal indenter, Tauern Window (Eastern Alps). Tectonics 36(6):1053–1071. https://doi.org/10.1002/2016TC004448

Froitzheim N, Schmid S, Conti P (1994) Repeated change from crustal shortening to orogen-parallel extension in the Austroalpineunits of Graubünden. Eclogae Geol Helv 87(2):559–612

Frasl G (1958) Zur Seriengliederung der Schieferhülle in den mittleren Hohen Tauern. Jahrb Geol Bundesanst 101:323–472

Frasl G, Frank W (1966) Einführung in die Geologie und Petrographie des Penninikums im Tauernfenster mit besonderer Berücksichtigung des Mittelabschnittes im Oberpinzgau, Land Salzburg. Der Aufschluss, Sonderheft 15:30–58

Frisch W (1968) Zur Geologie des Gebietes zwischen Tuxbach und Tuxer Hauptkamm bei Lanersbach (Zillertal, Tirol). Mitt Ges Geol Bergbaustud 18:287–336

Frisch W (1974) Die stratigraphisch-tektonische Gliederung der Schieferhülle und die Entwicklung des penninischen Raumes im westlichen Tauernfenster (Gebiet Brenner-Gerlospaß). Mitt Geol Ges Wien 66(67):9–20

Frisch W (1977) Der alpidische Internbau der Venedigerdecke im westlichen Tauernfenster. Neues Jahrb Geol Palaontol Monatsh 11:675–696

Frisch W (1980) Post-Hercynian formations of the western Tauern Window: sedimentological features, depositional environment, and age. Mitt Osterr Geol Ges 71(72):49–63

Frisch W, Dunkl I, Kuhlemann J (2000) Post-collisional orogen-parallel large-scale extension in the Eastern Alps. Tectonophysics 327(3–4):239–265. https://doi.org/10.1016/S0040-1951(00)00204-3

Fügenschuh B, Seward D, Mancktelow N (1997) Exhumation in a convergent orogen: the western Tauern window. Terra Nova 9(5–6):213–217

Fügenschuh B, Mancktelow NS, Schmid SM (2012) Comment on Rosenberg and Garcia: estimating displacement along the Brenner Fault and orogen-parallel extension in the Eastern Alps. Int J Earth Sci 101:1451–1455. https://doi.org/10.1007/s00531-011-0725-4

Geosphere Austria (2017) Multithematische geologische Karte von Österreich 1:1.000.000. https://geolba.maps.arcgis.com/apps/webappviewer/index.html?id=0e19d373a13d4eb19da3544ce15f35ec. Accessed 27 Nov 2023

Groß P, Handy MR, John T, Pestal G, Pleuger J (2020) Crustal-scale sheath folding at HP conditions in an exhumed Alpine subduction zone (Tauern Window, Eastern Alps). Tectonics 39(2):e2019TC005942. https://doi.org/10.1029/2019TC005942

Groß P, Pleuger J, Handy MR, Germer M, John T (2021) Evolving temperature field in a fossil subduction channel during the transition from subduction to collision (Tauern Window, Eastern Alps). J Metamorph Geol 39(2):247–269. https://doi.org/10.1111/jmg.12572

Groß P, Pleuger J, Handy MR (2022) Rift-related paleogeography of the European margin in the Eastern Alps (Central Tauern Window). Swiss J Geosci 115(1):1–40. https://doi.org/10.1186/s00015-022-00426-9

Handy MR (2025) Orogenic structure and topography track subduction singularities during slab delamination and detachment. Sci Rep 15:12091. https://doi.org/10.1038/s41598-025-94789-2

Handy MR, Babist J, Wagner R, Rosenberg C, Konrad M (2005) Decoupling and its relation to strain partitioning in continental lithosphere: insight from the Periadriatic fault system (European Alps). Geol Soc Lond Spec Publ 243(1):249–276. https://doi.org/10.1144/GSL.SP.2005.243.01.17

Handy MR, Schmid SM, Bousquet R, Kissling E, Bernoulli D (2010) Reconciling plate-tectonic reconstructions of Alpine Tethys with the geological–geophysical record of spreading and subduction in the Alps. Earth-Sci Rev 102(3–4):121–158. https://doi.org/10.1016/j.earscirev.2010.06.002

Höck V, Koller F (1989) Magmatic evolution of the Mesozoic ophiolites in Austria. Chem Geol 77(3–4):209–227

Hoschek G (2001) Thermobarometry of metasediments and metabasites from the Eclogite zone of the Hohe Tauern, Eastern Alps, Austria. Lithos 59(3):127–150. https://doi.org/10.1016/S0024-4937(01)00063-9

Hoschek G (2004) Comparison of calculated PT pseudosections for a kyanite eclogite from the Tauern Window, Eastern Alps, Austria. Eur J Mineral 16(1):59–72. https://doi.org/10.1127/0935-1221/2004/0016-0059

Jozi Najafabadi A, Haberland C, Le Breton E, Handy MR, Verwater VF, Heit B et al (2022) Constraints on crustal structure in the vicinity of the Adriatic Indenter (European Alps) from Vp and Vp/Vs local earthquake tomography. J Geophys Res Solid Earth 127(2):e2021JB023160. https://doi.org/10.1029/2021JB023160

Jozi Najafabadi A, Haberland C, Handy MR, Le Breton E, Weber M (2023) Seismic wave attenuation (1/Qp) in the crust underneath the Eastern and eastern Southern Alps (Europe): imaging effects of faults, fractures, and fluids. Earth Planets Space 75(1):187. https://doi.org/10.1186/s40623-023-01942-0

Klotz T, Pomella H, Reiser M, Fügenschuh B, Zattin M (2019) Differential uplift on the boundary between the Eastern and the Southern European Alps: thermochronologic constraints from the Brenner Base Tunnel. Terra Nova 31(3):281–294. https://doi.org/10.1111/ter.12398

Koller F, Prestal G (2003) Die ligurischen Ophiolite der Tarntaler Berge und der Matreier Zone. Arbeitstagung der Geologische Bundesanstalt Blatt 148:65–76

Kreuss O (2013) Geologische Karte der Republik Österreich 1:50.000—GEOFAST (Blatt 176 Mühlbach). Geologische Bundesanstalt, Wien

Kreuss O (2018) Geologische Karte der Republik Österreich 1:50.000—GEOFAST (Blatt 149 Lanersbach). Geologische Bundesanstalt, Wien

Lammerer B (1986) Das Autochthon im westlichen Tauernfenster. Jahrb Geol Bundesanst 129:51–67

Lammerer B, Weger M (1998) Footwall uplift in an orogenic wedge: the Tauern Window in the Eastern Alps of Europe. Tectonophysics 285(3–4):213–230. https://doi.org/10.1016/S0040-1951(97)00272-2

Lammerer B, Gebrande H, Lüschen E, Veselá P (2008) A crustal-scale cross-section through the Tauern Window (eastern Alps) from geophysical and geological data. Geol Soc Lond Spec Publ 298(1):219–229. https://doi.org/10.1144/SP298.11

Laubscher HP (1971) Das Alpen-Dinariden-Problem und die Palinspastik der südlichen tethys. Geol Rundsch 60(3):813–833

Le Breton E, Handy MR, Molli G, Ustaszewski K (2017) Post-20 Ma motion of the Adriatic Plate: new constraints from surrounding orogens and implications for crust-mantle decoupling. Tectonics 36(12):3135–3154. https://doi.org/10.1002/2016TC004443

Linzer HG, Decker K, Peresson H, Dell'Mour R, Frisch W (2002) Balancing lateral orogenic float of the Eastern Alps. Tectonophysics 354(3–4):211–237. https://doi.org/10.1016/S0040-1951(02)00337-2

Lüschen E, Lammerer B, Gebrande H, Millahn K, Nicolich R, TRANSALP Working Group (2004) Orogenic structure of the Eastern Alps, Europe, from TRANSALP deep seismic reflection profiling. Tectonophysics 388(1–4):85–102. https://doi.org/10.1016/j.tecto.2004.07.024

Lüschen E, Borrini D, Gebrande H, Lammerer B, Millahn K, Neubauer F et al (2006) TRANSALP—deep crustal vibroseis and

explosive seismic profiling in the Eastern Alps. Tectonophysics 414(1–4):9–38. https://doi.org/10.1016/j.tecto.2005.10.014
Luth S, Willingshofer E, Ter Borgh M, Sokoutis D, Van Otterloo J, Versteeg A (2013) Kinematic analysis and analogue modelling of the Passeier-and Jaufen faults: implications for crustal indentation in the Eastern Alps. Int J Earth Sci 102:1071–1090. https://doi.org/10.1007/s00531-012-0846-4
Mancktelow NS, Stöckli DF, Grollimund B, Müller W, Fügenschuh B, Viola G, Seward D, Villa IM (2001) The DAV and Periadriatic fault systems in the Eastern Alps south of the Tauern window. Int J Earth Sci 90:593–622. https://doi.org/10.1007/s005310000190
McPhee PJ, Handy MR (2024) Post-collisional reorganisation of the Eastern Alps in 4D – crust and mantle structure. Tectonics 43(8):e2024TC008374. https://doi.org/10.1029/2024TC008374
Moser M (2011) Geologische Karte der Republik Österreich 1:50.000—GEOFAST (Blatt 147 Axams). Geologische Bundesanstalt, Wien
Moser M (2012) Geologische Karte der Republik Österreich 1:50.000—GEOFAST (Blatt 174 Timmelsjoch). Geologische Bundesanstalt, Wien
Moser M, Pavlik W (2014) Geologische Karte der Republik Österreich 1:50.000—GEOFAST (Blatt 150 Mayrhofen). Geologische Bundesanstalt, Wien
Ortner H, Reiter F, Brandner R (2006) Kinematics of the Inntal shear zone–sub-Tauern ramp fault system and the interpretation of the TRANSALP seismic section, Eastern Alps, Austria. Tectonophysics 414(1–4):241–258. https://doi.org/10.1016/j.tecto.2005.10.017
Pennacchioni G, Mancktelow NS (2007) Nucleation and initial growth of a shear zone network within compositionally and structurally heterogeneous granitoids under amphibolite facies conditions. J Struct Geol 29(11):1757–1780. https://doi.org/10.1016/j.jsg.2007.06.002
Pomella H, Klötzli U, Scholger R, Stipp M, Fügenschuh B (2011) The northern Giudicarie and the Meran-Mauls fault (Alps, Northern Italy) in the light of new paleomagnetic and geochronological data from boudinaged Eo-/Oligocene tonalites. Int J Earth Sci 100:1827–1850. https://doi.org/10.1007/s00531-010-0612-4
Pomella H, Stipp M, Fügenschuh B (2012) Thermochronological record of thrusting and strike-slip faulting along the Giudicarie fault system (Alps, Northern Italy). Tectonophysics 579:118–130. https://doi.org/10.1016/j.tecto.2012.04.015
Pomella H, Flöss D, Speckbacher R, Tropper P, Fügenschuh B (2016) The western end of the Eoalpine High-Pressure Belt (Texel unit, South Tyrol/Italy). Terra Nova 28(1):60–69. https://doi.org/10.1111/ter.12191
Pomella H, Costantini D, Aichholzer P, Reiser M, Schuster R, Tropper P (2022) Petrological and geochronological investigations on the individual nappes of the Meran-Mauls nappe stack (Austroalpine unit/South Tyrol, Italy). Austrian J Earth Sci 115(1):15–40. https://doi.org/10.17738/ajes.2022.0002
Prey S (1980) Die Geologie Österreichs in ihrem heutigen geodynamischen Entwicklungstand sowie die geologischen Bauteile und ihre Zusammenhänge. In: Oberhauser R (ed) Der Geologische Aufbau Österreichs. Springer, Wien, pp 79–117
Prey S (1989) Ein steilstehendes Störungssystem als Westbegrenzung des Tauernfensters. J Geol BA 132(Heft 4 Suppl):745–749
Ratschbacher L, Merle O, Davy P, Cobbold P (1991a) Lateral extrusion in the Eastern Alps, part 1: boundary conditions and experiments scaled for gravity. Tectonics 10(2):245–256. https://doi.org/10.1029/90TC02622
Ratschbacher L, Frisch W, Linzer HG, Merle O (1991b) Lateral extrusion in the Eastern Alps, part 2: structural analysis. Tectonics 10(2):257–271. https://doi.org/10.1029/90TC02623
Reiter F, Freudenthaler C, Hausmann H, Ortner H, Lenhardt W, Brandner R (2018) Active seismotectonic deformation in front of the Dolomites indenter, Eastern Alps. Tectonics 37(12):4625–4654. https://doi.org/10.1029/2017TC004867
Ricchi E, Bergemann CA, Gnos E, Berger A, Rubatto D, Whitehouse MJ, Walter F (2020) Cenozoic deformation in the Tauern Window (Eastern Alps) constrained by in situ Th-Pb dating of fissure monazite. Solid Earth 11(2):437–467. https://doi.org/10.5194/se-11-437-2020
Rockenschaub M, Nowotny A (2009) Geologische Karte der Republik Österreich 1:50.000 (Blatt 148 Brenner). Geologische Bundesanstalt, Wien
Rockenschaub M, Kolenprat B, Nowotny A (2003) Das westliche Tauernfenster. Arbeitstagung der Geologische Bundesanstalt Blatt 148:7–38
Rockenschaub M, Nowotny A, Brandner R, Fenti V, Frisch W, Friz C et al. (2011) Geologische Karte der Republik Österreich 1:50.000 (Blatt 175 Sterzing). Geologische Bundesanstalt, Wien
Rosenberg CL, Berger A (2009) On the causes and modes of exhumation and lateral growth of the Alps. Tectonics. https://doi.org/10.1029/2008TC002442
Rosenberg CL, Garcia S (2011) Estimating displacement along the Brenner Fault and orogen-parallel extension in the Eastern Alps. Int J Earth Sci 100:1129–1145. https://doi.org/10.1007/s00531-011-0645-3
Rosenberg CL, Garcia S (2012) Reply to the comment of Fügenschuh et al. on the paper 'Estimating displacement along the Brenner Fault and orogen-parallel extension in the Eastern Alps' by Rosenberg and Garcia, Int J Earth Sci (Geol Rundsch) (2011) 100:1129–1145. Int J Earth Sci 101:1457–1464. https://doi.org/10.1007/s00531-011-0726-3
Rosenberg CL, Schneider S (2008) The western termination of the SEMP fault (eastern Alps) and its bearing on the exhumation of the Tauern Window. Geol Soc Lond Spec Publ 298(1):197–218. https://doi.org/10.1144/SP298.10
Rosenberg CL, Brun JP, Gapais D (2004) Indentation model of the Eastern Alps and the origin of the Tauern Window. Geology 32(11):997–1000. https://doi.org/10.1130/G20793.1
Rosenberg CL, Brun JP, Cagnard F, Gapais D (2007) Oblique indentation in the Eastern Alps: insights from laboratory experiments. Tectonics 26:TC2003. https://doi.org/10.1029/2006TC001960
Rosenberg CL, Berger A, Bellahsen N, Bousquet R (2015) Relating orogen width to shortening, erosion, and exhumation during Alpine collision. Tectonics 34(6):1306–1328
Rosenberg CL, Schneider S, Scharf A, Bertrand A, Hammerschmidt K, Rabaute A, Brun JP (2018) Relating collisional kinematics to exhumation processes in the Eastern Alps. Earth-Sci Rev 176:311–344
Rudmann JB, Tanner DC, Stipp M, Pomella H, Brandes C (2025) 2-D kinematic restoration of the western Tauern Window, Eastern Alps using thermochronological and P-T constraints. Tectonics 44:e2024TC008371. https://doi.org/10.1029/2024TC008371
Scharf A, Handy MR, Favaro S, Schmid SM, Bertrand A (2013) Modes of orogen-parallel stretching and extensional exhumation in response to microplate indentation and roll-back subduction (Tauern Window, Eastern Alps). Int J Earth Sci 102:1627–1654. https://doi.org/10.1007/s00531-013-0894-4
Schmid SM, Pfiffner OA, Froitzheim N, Schönborn G, Kissling E (1996) Geophysical-geological transect and tectonic evolution of theSwiss-Italian Alps. Tectonics 15(5):1036–1064. https://doi.org/10.1029/96TC00433
Schmid SM, Fügenschuh B, Kissling E, Schuster R (2004) Tectonic map and overall architecture of the Alpine orogen. Eclogae Geol Helv 97:93–117. https://doi.org/10.1007/s00015-004-1113-x

Schmid SM, Scharf A, Handy MR, Rosenberg CL (2013) The Tauern Window (Eastern Alps, Austria): a new tectonic map, with cross-sections and a tectonometamorphic synthesis. Swiss J Geosci 106(1):1–32. https://doi.org/10.1007/s00015-013-0123-y

Schmidegg O (1953) Die Silltalstörung und das Tonvorkommen bei der Stefansbrücke. Verhandlungen der geologischen Bundesanstalt, Heft 2:135–138

Schmidegg O (1954) Achsen-und Flächengefüge beiderseits des Silltalbruches zwischen Innsbruck und Matrei. Tschermaks Mineral Petrogr Mitt 4:125–137

Schneider S (2015) Exhumation mechanisms of middle and lower crust in the western Tauern Window, Eastern Alps. Dissertation, Freie Universität Berlin

Schönborn G (1999) Balancing cross sections with kinematic constraints: the Dolomites (northern Italy). Tectonics 18(3):527–545. https://doi.org/10.1029/1998TC900018

Selverstone J (1985) Petrologic constraints on imbrication, metamorphism, and uplift in the SW Tauern Window, Eastern Alps. Tectonics 4(7):687–704. https://doi.org/10.1029/TC004i007p00687

Selverstone J (1988) Evidence for east-west crustal extension in the Eastern Alps: implications for the unroofing history of the Tauern Window. Tectonics 7(1):87–105

Spada M, Bianchi I, Kissling E, Agostinetti NP, Wiemer S (2013) Combining controlled-source seismology and receiver function information to derive 3-D Moho topography for Italy. Geophys J Int 194(2):1050–1068. https://doi.org/10.1093/gji/ggt148

Staub R (1924) Der Bau der Alpen—Versuch einer Synthese. Beiträge zur geologischen Karte der Schweiz (52, N. F. 82). Francke, Bern

Stipp M, Fügenschuh B, Gromet LP, Stünitz H, Schmid SM (2004) Contemporaneous plutonism and strike-slip faulting: A case study from the Tonale fault zone north of the Adamello pluton (Italian Alps). Tectonics 23(3):TC3004. https://doi.org/10.1029/2003TC001515

Thiele O (1980) Das Tauernfenster. In: Oberhauser R (ed) Der Geologische Aufbau Österreichs. Springer, Wien, pp 300–314

Töchterle A, Brandner R, Reiter F (2007) Geologisches Tiefenprofil 1:100.000 entlang der Trasse des geplanten Brenner-Basistunnels. Posterbeilage im Tagungsband „BBT 2007“, Internationales Symposium Brenner Basistunnel und Zulaufstrecken, 1. März 2007, Innsbruck

Töchterle A, Brandner R, Reiter F (2011) Strain partitioning on major fault zones in the northwestern Tauern Window – insights from the investigations of the Brenner base tunnel. Austrian J Earth Sci 104(1):15–35

TRANSALP Working Group, Gebrande H, Lüschen E, Bopp M, Bleibinhaus F, Lammerer B et al (2002) First deep seismic reflection images of the Eastern Alps reveal giant crustal wedges and transcrustal ramps. Geophys Res Lett 29(10):1452. https://doi.org/10.1029/2002GL014911

Verwater VF, Le Breton E, Handy MR, Picotti V, Jozi Najafabadi A, Haberland C (2021) Neogene kinematics of the Giudicarie Belt and eastern Southern Alpine orogenic front (northern Italy). Solid Earth 12:1309–1334. https://doi.org/10.5194/se-12-1309-2021

Veselá P, Lammerer B (2008) The Pfitsch-Mörchner Basin, an example of the post-Variscan sedimentary evolution in the Tauern Window (Eastern Alps). Swiss J Geosci 101:73–88. https://doi.org/10.1007/s00015-008-1293-x

Veselá P, Lammerer B, Wetzel A, Söllner F, Gerdes A (2008) Post-variscan to early Alpine sedimentary basins in the Tauern window (eastern Alps). Geol Soc Lond Spec Publ 298(1):83–100. https://doi.org/10.1144/SP298.5

Veselá P, Söllner F, Finger F, Gerdes A (2010) Magmato-sedimentary Carboniferous to Jurassic evolution of the western Tauern window, Eastern Alps (constraints from U-Pb zircon dating and geochemistry). Int J Earth Sci 100:993–1027. https://doi.org/10.1007/s00531-010-0596-0

Veselá P, Oriolo S, Basei MAS, Lammerer B, Siegesmund S (2022) The detrital zircon record of Variscan to post-Variscan tectono-sedimentary and magmatic processes in the Tauern Window (Eastern Alps). Int J Earth Sci 111(4):1273–1287. https://doi.org/10.1007/s00531-022-02179-0

Villani F, Antonioli A, Pastori M, Baccheschi P, Ciaccio MG (2024) Stress patterns and crustal anisotropy in the Eastern Alps: Insightsfrom seismological and geological observations. Tectonics 43(3):e2023TC008033. https://doi.org/10.1029/2023TC008033

Viola G, Mancktelow NS, Seward D (2001) Late Oligocene-Neogene evolution of Europe-Adria collision: new structural and geochronological evidence from the Giudicarie fault system (Italian Eastern Alps). Tectonics 20(6):999–1020. https://doi.org/10.1029/2001TC900021

Wolff R, Hetzel R, Dunkl I, Anczkiewicz AA, Pomella H (2020) Fast cooling of normal-fault footwalls: rapid fault slip or thermal relaxation? Geology 48(4):333–337. https://doi.org/10.1130/G46940.1

Wolff R, Hetzel R, Dunkl I, Anczkiewicz AA (2021) New constraints on the exhumation history of the western Tauern Window (European Alps) from thermochronology, thermokinematic modeling, and topographic analysis. Int J Earth Sci 110(8):2955–2977. https://doi.org/10.1007/s00531-021-02094-w

Wolff R, Wölfler A, Hampel A, Dunkl I (2024) Constraining the slip history of the Katschberg normal fault (Eastern Tauern Window) by thermo-kinematic modeling: implications for the tectonic evolution of the Eastern European Alps in the late Cenozoic. Tectonophysics 890:230514. https://doi.org/10.1016/j.tecto.2024.230514

Wölfler A, Wolff R, Hampel A, Hetzel R, Dunkl I (2023) Phases of enhanced exhumation during the Cretaceous and Cenozoic orogenies in the Eastern European Alps: new insights from thermochronological data and thermokinematic modeling. Tectonics 42:e2022TC007698. https://doi.org/10.1029/2022TC007698